DEVELOPMENT OF A MEVVA BASED BERYLLIUM–7 PLASMA SOURCE

by

David K. Olson

A thesis submitted to the faculty of

Brigham Young University

in partial fulfillment of the requirements for the degree of

Master of Science

Department of Physics and Astronomy

Brigham Young University

August 2007

BRIGHAM YOUNG UNIVERSITY

GRADUATE COMMITTEE APPROVAL

of a thesis submitted by

David K. Olson

This thesis has been read by each member of the following graduate committee and by majority vote has been found to be satisfactory.

Date	Bryan G. Peterson, Chair
Date	Grant W. Hart
Date	David D. Allred

BRIGHAM YOUNG UNIVERSITY

As chair of the candidate's graduate committee, I have read the thesis of David K. Olson in its final form and have found that (1) its format, citations, and bibliographical style are consistent and acceptable and fulfill university and department style requirements; (2) its illustrative materials including figures, tables, and charts are in place; and (3) the final manuscript is satisfactory to the graduate committee and is ready for submission to the university library.

Date

Bryan G. Peterson
Chair, Graduate Committee

Accepted for the Department

Ross L. Spencer, Department Chair
Department of Physics and Astronomy

Accepted for the College

Thomas W. Sederberg, Associate Dean
College of Mathematics and Physical Sciences

ABSTRACT

DEVELOPMENT OF A MEVVA BASED BERYLLIUM–7

PLASMA SOURCE

David K. Olson

Department of Physics and Astronomy

Master of Science

We have designed a new type of plasma gun ion source for a Malmberg–Penning trap based on Metal Vapor Vacuum Arc (MeVVA) ion source designs. Our primary intent with this MeVVA–type source is to create a confinable beryllium-7 (^{7}Be) plasma. ^{7}Be is a peculiar isotope due to its varying radioactive decay half-life in different electro-chemical configurations. It is also found in an unexpected abundance at high altitudes of the Earth's atmosphere. It is possible ioniziation affects the radioactivity of the isotope, partly explaining this discrepancy with atmospheric models. The short half-life of ^{7}Be requires us to replace the sample inside the ion source on a regular basis. Our design makes it possible to easily remove the cathode of the ion source from an ultra-high vacuum trap and exchange ^{7}Be samples while only needing to repressurize a small chamber rather than the entire trap. This design has an added benefit of being capable of generating plasmas from a wide variety of metals by sim-

ply exchanging the source target in the removable cathode. Because of this wide compatibility, we will be able to use our trap for studying any number of different plasmas, including other radioactive types. Testing of the ion source design shows we are able to extract more than a sufficient number of ions at reasonable energies for confinement.

ACKNOWLEDGMENTS

I would like to express a great deal of appreciation to my research advisors Dr. Peterson and Dr. Hart for their help in making this research successful. Dr. Allred's input and provision of materials for performing the optical tests was also of major import to this work. A large part of the research into understanding how to design, build, and understand a MeVVA source was done with the help of Ian G. Brown of Lawrence Berkeley National Laboratory. Ian is the original developer of the MeVVA source, and his counsel in designing this variation has been immensely helpful. The SEM work and photographs were done with the help of my friend Felipe Rivera of Brigham Young University. His expertise in the finer adjustments of the SEM has allowed us to get excellent photographs of the target surface. His efforts in analyzing the crystal structure are also greatly appreciated. Finally, I am very grateful to my family and friends who have encouraged me throughout my schooling and research. Their continued support will build me through the remainder of my education and into my career.

Funding for this project was provided in part by the Rocky Mountain NASA Space Grant Consortium.

Contents

List of Tables

List of Figures

Chapter 1

Introduction

Ion sources have become common in scientific and industrial use, enough so that ion source research is almost considered to be its own field. Those privy to this field have been known to refer to it jokingly, though only partially so, as "ion sourcery". Although we have been able to create a large number of types of ion sources and their use can range from small power sources to larger current beam sources, a great deal of the physics behind their function is still unknown. In some specialized projects, a new type of ion source may even need to be developed.

Creating an ion source for radioactive metals poses some particular difficulties with many currently established ion source designs. Our research will use the beryllium-7 (^{7}Be) ion, which has a half-life on the order of a couple of months. This half-life is long enough that we can make use of a solid sample from which we can extract ions, but short enough that typical source configurations are useful only for a brief time.

As an apprentice in this field, I have developed a modified version of a common type of ion source that is suitable for the ^{7}Be isotope. The modifications are also beneficial in that the design allows the same equipment to be used as a source of ions from a large number of other conductive materials. The ion source we have

constructed will be used in answering some questions about the behavior of the ^{7}Be ion by studying a non-neutral ^{7}Be plasma. This thesis details the design and behavior of this new ion source.

1.1 ^{7}Be

The ^{7}Be isotope is interesting and important for many reasons. In addition to being the lightest known isotope that solely undergoes electron capture β-decay, it is also one of the intermediate products in the fusion processes in the sun. ^{7}Be has a half-life of roughly 53 days.

^{7}Be is also present in our atmosphere. It is created by means of spallation reactions of cosmic rays with oxygen or nitrogen molecules.[1] The atoms are carried through atmospheric transport by binding with heavier aerosol particles.[2] Peak production of ^{7}Be occurs at an altitude of 20 km, where cosmic ray flux and atmospheric density maximize the number of spallation reactions. The density of ^{7}Be at this height is about 10^3 atoms per gram of air.[3] Current models suggest this ratio should remain constant at higher altitudes, and studies have confirmed this suggestion in the lower stratosphere.[3]

^{7}Be oxidizes rapidly in the lower atmosphere. The aerosol particles ^{7}Be attaches to often become condensation nuclei for cloud formation, and so the ^{7}Be atoms are removed from the atmosphere and reach the surface of the earth through rainfall. The entire cycle from creation to rainfall removal is a period of 35–40 days, a little less than one half-life.[4] Because of its movement through the atmosphere and removal by rain, scientists have found ^{7}Be to be an excellent medium–term tracer in weather patterns and erosional trends.[5–7]

The decay of ^{7}Be is usually associated with the release of only a 0.9 MeV electron

(89.5%)	$^7Be + e^- \rightarrow {}^7Li + \nu_e$	0.861 MeV e^- neutrino
(10.5%)	$^7Be + e^- \rightarrow {}^7Li + \gamma + \nu_e$	0.383 MeV e^- neutrino
γ ray	0.478 MeV	
UV photon	62.2 eV	(Result of electron transition to innermost orbital)

Table 1.1 Radioactive decay of the ^{7}Be atom.

neutrino. 10.5% of the decays, however, follow a different decay route, releasing a 0.4 MeV neutrino along with a 0.5 MeV γ-ray photon. Capture of an inner shell electron (K shell) can result in a 62 eV UV photon from a cascading electron (See table 1.1.) Voytas et al. established that K shell electron capture occurs 96% of the time, while L shell capture only occurs 4% of the time.[8] This measured rate is significantly different from previous theory, but Ray et al. showed that the discrepancy is due to the electrochemical configuration.[9]

Because of the difficulty in neutrino detection, measuring the half-life of the ^{7}Be atom requires detection of emissions that do not occur in every decay. UV photon emission occurs at an energy that is also difficult to detect. However, the rate of γ ray emission has been well established, and the γ ray is typically the detected emission in precise half-life measurements of ^{7}Be.

One of the more curious properties of the ^{7}Be atom is that the half-life of ^{7}Be is affected by its electrochemical configuration—binding to other atoms actually changes the rate of radioactive decay by a small amount.[10,11] As the only type of radioactive decay in ^{7}Be is electron capture, it is easy to imagine that by completely ionizing a ^{7}Be atom, we can stop its decay completely. The half-life's dependence on electrochemical configuration implies that we might expect the half-life of ^{7}Be to increase with even

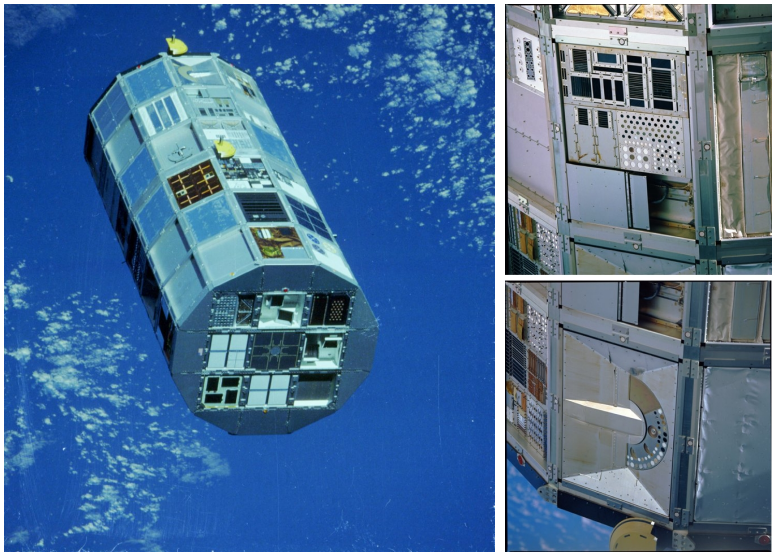

Figure 1.1 The LDEF satellite. A close view shows the panels installed on the ends of the satellite. These panels found large quantities of ^{7}Be at orbital altitudes.

partial ionization, because the electrons will be held in a stronger potential. Ionization has more of an effect on this potential than bonding with other atoms, and so we might even expect the increase in half-life to be more significant than the changes seen in chemical bonding.

1.2 The Long Duration Exposure Facility

The Long Duration Exposure Facility (LDEF) was a research satellite placed by the STS-41-C space shuttle flight in April, 1984. This facility consisted of a number of plates and sections designed to analyze the effects of long-term exposure to orbital altitude conditions on the materials used in building spacecraft. (Fig. 1.1) The LDEF was retrieved by NASA in 1990, and their analysis of the leading end panels found that the concentration of ^{7}Be at an altitude of 300 km was 3.8×10^{6} atoms per gram of air, three to four orders of magnitude greater than the atmospheric models predicted.[12]

Initial theories to explain this finding included an unknown transfer mechanism bringing ^{7}Be from the lower to the upper atmosphere,[12] transport from the sun by solar flare activity,[13] or gravitational fractionation.[14] In a followup paper, it is suggested that though solar flux could contribute to the amount of ^{7}Be in our atmosphere, the quantity is minimal in comparison to the amount created by means of cosmic ray spallation.[15] The assumptions made in the gravitational model include ^{7}Be being present as a free atom, rather than bonded to oxygen, fluorine, or aerosol particles as we would expect. This assumption would need to be examined and more strongly established for the model to be credible.

These arguments lead us to believe the presented theories are unsatisfactory in explaining the amount of ^{7}Be in our atmosphere. However, given the behavior of the ^{7}Be atom's radioactive decay in its various electrochemical configurations, the possibility of changing its half-life significantly by ionizing the atom might help explain NASA's finding. High energy cosmic rays do create ^{7}Be as an ion. If the ion is able to remain ionized for a longer lifetime at high altitudes, where collisions are infrequent, it might have a different half-life than expected. A significant increase in the half-life of the isotope in an ionized state might, at least partially, explain the large amount of ^{7}Be found by the LDEF satellite.

1.3 Ion Confinement and Detection

Measuring the half-life of an ion requires special techniques. Ions can be confined relatively easily by using a Malmberg–Penning trap for non-neutral plasmas.[16] The Malmberg–Penning trap configuration is ideal for confining the ions for long enough periods of time to make the measurement. This trap configuration is simply a type of Penning trap using a solenoid magnetic field with applied voltages at the ends.

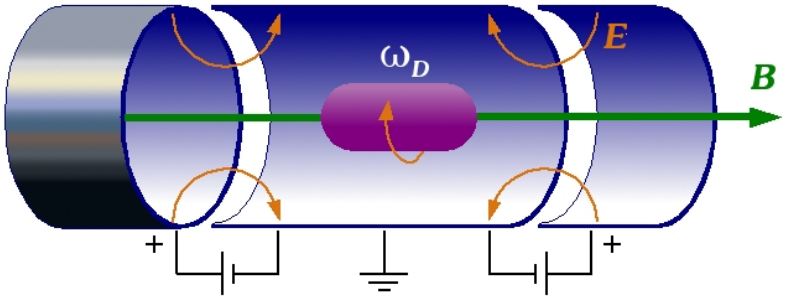

Figure 1.2 Basic design of a Malmberg–Penning trap.

(Fig. 1.2) The magnetic field confines the plasma radially while the voltage plates apply axial confinement. This type of trap is designed to confine only one species of charge, and so electrons are not present in the ion plasma. The ions in a Malmberg–Penning trap do not experience recombination since the electrons are not present, and so the plasma has a long lifetime. The Malmberg–Penning trap has been used in research facilities across the world for a while, and it has proven to be an effective means of plasma study.[17]

Detecting the radiation of a ^{7}Be ion poses a unique problem. The geometry of a Malmberg–Penning trap severely limits the solid angle available for γ ray detection. In addition, any ^{7}Be that has touched the grounded wall will have neutralized, and would decay at the normally expected rate. The decay of the unionized atoms could introduce error in trying to measure a change in the half-life of ionized atoms. The configuration of the trap does, however, provide another effective method of measuring radioactive decay not by detecting emissions, but by detecting the concentrations of ^{7}Be and its daughter atom ^{7}Li directly.

Because the ions will undergo cyclotron motion in the magnetic field, the resulting electrical signal from the accelerating charges can be used to measure the amounts

$^{10}B \ + \ p^{+} \rightarrow \ ^{7}Be \ + \ \alpha$
α particle energy is dependent on incident proton energy.

Table 1.2 Reaction by which ^{7}Be can be created from ^{10}B.

of ^{7}Be and ^{7}Li by means of Fourier–Transform Ion Cyclotron Mass Spectroscopy (FT–ICR/MS).[18] The cyclotron frequency is mass-dependent, allowing us to distinguish between the two ions. However, the masses of the ions in this decay differ by only 0.09%, requiring a 0.5 T magnetic field with fluctuations smaller than 50 μT for a plasma at 5% of the Brillouin limit. This trap has been assembled at Brigham Young University and shown to have magnetic fields of this constancy.[19]

1.4 MeVVA Ion Sources

Creating an ion source for this system is a greater challenge, and the primary subject of this thesis. ^{7}Be can be created in a laboratory by proton bombardment of a boron-10 sample (Table 1.2).[20] We have developed a method of creating a spot of ^{7}Be on a sample of ^{10}B enriched boron carbide using a proton accelerator. Because beryllium and boron carbide are conductive, extracting the ^{7}Be from the boron carbide is possible by means of a technique developed for the Metal Vapor Vacuum Arc (MeVVA) ion source.[21]

The MeVVA ion source provides a substantial current of metal ions without requiring inordinate power consumption. A MeVVA source puts a high voltage between two plates. A solid sample of the metal to be ionized is attached to one of these plates (the cathode). Typically the sample is attached to the face of the cathode plate with a conductive cement. A high voltage discharge is triggered to create a high energy arc

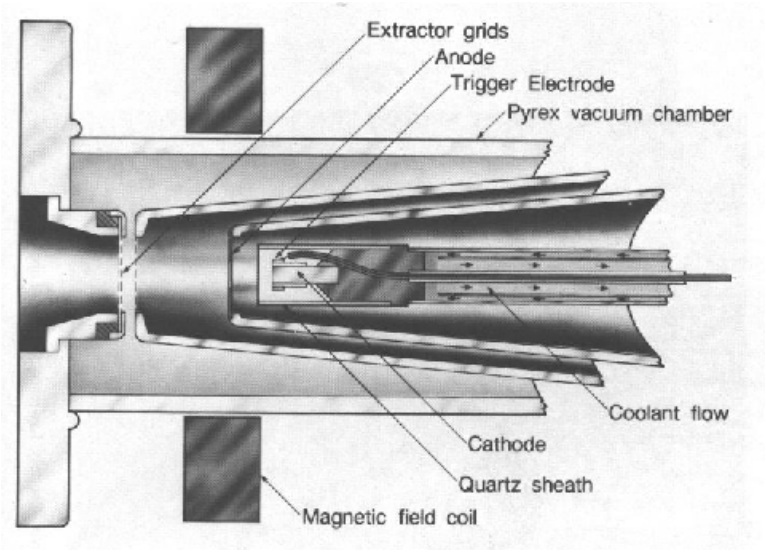

Figure 1.3 Schematic of a basic MeVVA Ion Source. Figure taken from The Physics and Technology of Ion Sources, Ian G. Brown (Wiley, New York, 1989).

between the two plates from minute regions called "cathode spots". These regions can reach current densities of more than 10^6 A/cm^2. The high energy from the arc ablates and ionizes the metal sample. The ions in the quasi-neutral plasma created by the arc are accelerated toward the other plate (the anode). A hole in the center of the anode allows them to pass through into an extraction mechanism, which turns the stream of particles into an ion beam.[21] The extractor is essentially a set of grids that removes the free electrons and refines the ion beam. The beam can be sustained by simply triggering multiple arcs in succession to sustain the release of ions from the source. (See Figure 1.3.)

Ion sources like the MeVVA source are often characterized by various parameters that affect the quality of ion beam produced. Some of these parameters include the current that passes through the arc plates to generate the plasma, the voltage applied to the extractor grids, and the spacing between the grids inside the extraction

mechanism. The best quality (highest current) of ion beam we can get from an ion source is governed by the Child-Langmuir law.[23,24] This law gives us the maximum current density (j) in the ion beam as a function of ion charge state (ζ), the ion mass in amu (A), the extraction voltage in kV (U) and the extraction gap width in cm (d):

$$j = 1.72\frac{(\frac{\zeta}{A})^{\frac{1}{2}}U^{\frac{3}{2}}}{d^2} \tag{1.1}$$

MeVVA sources have typically been placed in an evacuated Pyrex cylinder. The cathode is usually equipped with a cooling system because of the heat generated by electrical arcing across the plates when multiple shots are taken. (A shot is a single arc or spark between the plates.) Generating the arcs requires a custom power supply external to the source. High current, short time scale pulses in the electronics of the source also require some precaution with radio-frequency signals radiating from the wiring. Typically, good quality coaxial cable is used to minimize this radiation in addition to RF shielding the power supply.[25–31]

1.5 Building a New Ion Source

The MeVVA design provides a relatively simple mechanism for removing and ionizing the ^{7}Be from a boron carbide sample. The characteristics of ^{7}Be and of a Malmberg–Penning trap require a unique approach to such a source, however, and our design includes some innovative modifications, in addition to a number of simplifications, to achieve its particular function. The following chapters describe the particulars of the source's design and its behavior observed through extensive testing. The results of this work show that our ion source is sufficient for use in studying a ^{7}Be plasma, as well as flexible for other research projects that can be done at Brigham Young University.

Chapter 2

Development of the modified MeVVA

2.1 Project Requirements

Though the MeVVA technique is ideally suited for extraction of ^{7}Be from a boron carbide sample, the typical application of the technique is far from satisfactory for the experiment.

2.1.1 Considerations for the Trap Environment

To make an accurate measurement of a half-life on the order of two months, we need to be able to confine the plasma for roughly that length of time. The trap was designed using a copper magnet to remove the need to replace liquid helium in cryogenic magnets. In addition, ultra high vacuum conditions are needed to prevent recombination of the ions through collisions with neutral particles. Glues, plastics, and many other materials are not suitable for maintaining these pressures, so the source has to be designed with acceptable materials and without the use of cements.

High energy arcs typically impart a great deal of thermal energy to the ions they create. Extraction voltages further accelerate the ions, and so the typical MeVVA source would create ions with energies too high to confine easily in the trap. The source must be designed to create ions at energies low enough to confine.

2.1.2 Considerations for Radioactivity

The target sample of a MeVVA source is typically cemented to the cathode with a conductive cement. For these types of sources, the sample is permanently affixed, and replacing the material with another sample or with a different material is a difficult and possibly damaging process. During the course of an experiment, what ^{7}Be remains on the boron carbide target after extraction will continue to decay, thereby rendering the ion source useless for further experiments. The source design must then accommodate exchanging samples of ^{7}Be quickly and easily.

Due to the size of the trap, evacuating the entire system is a process that extends over periods on the order of a few weeks. During the time the vacuum pump brings the trap to an acceptable pressure level, the source will be decaying and have more lithium present to begin than we would like. To minimize the delay time between inserting the source and running the experiment, the trap is designed with a small access chamber that can be closed off from the rest of the trap. (Fig. 2.1) This chamber is small enough that the evacuation time is on the order of hours. The source must be able to fit into the small chamber, and also be easily handled while inside the trap. The source must be easily removed from its position after use and quick to re-insert with a new target for the next experiment.

A removable source introduces the issue of maintaining good electrical contact. As we are dealing with high currents, resistances need to be kept low to prevent excessive heating of the system. Arcs need to be restricted to just the expected area,

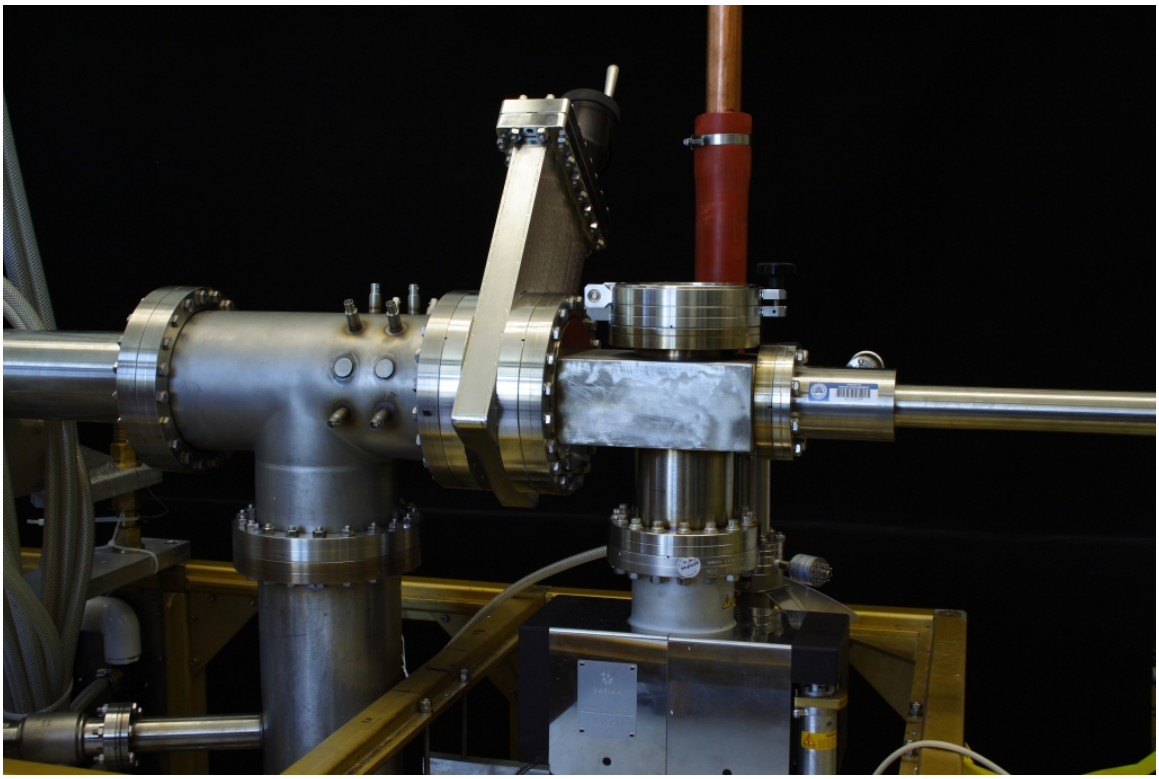

Figure 2.1 The access chamber for the trap. The mounting rings sit on the left end of the large T in the photo. The manipulator arm extends to the right.

so good, solid electrical contacts inside the trap are essential. The trap is equipped with a rack and pinion style manipulator, which can be used for removal and insertion. However, the only motion available with the manipulator is back and forth along the axis of the trap, and so any mechanism for securing the source and applying electrical contact must be usable with minimal motion. Typically these sources use a cylindrical symmetry, which lends itself well to this restriction.

2.1.3 Considerations for ^{7}Be Availability

As stated previously, ^{7}Be is obtainable by striking a ^{10}B atom in a boron carbide target with a proton beam. The beam creates only a small spot of ^{7}Be in a region on the boron carbide surface. The mechanism by which cathode spots form in arc discharge remains unknown, and so arcs may occur anywhere along the surface adjacent to the where the arc trigger is initiated. In order to make the source efficient, a mask must be applied to restrict the vacuum arcs to the region where the ^{7}Be has been deposited, ensuring that a sufficient quantity of ^{7}Be is released in addition to the boron, carbon, and other materials used in the conductive parts of the source design.

The source must also be designed to prevent discharges from occurring elsewhere within the source. It must also be devoid of spaces where pockets of air could be trapped inside the source, creating low resistance paths for other arcs to occur in addition to virtual vacuum leaks. Such regions could also be dangerous, since an arc through the trapped gas could cause it to expand rapidly.

2.2 Design

Many of these issues have simple solutions. For example, choosing materials known to have good conductivity properties and good vacuum qualities for making the source

helps us to maintain a plasma long enough to take half-life measurements. For our source, we use oxygen-free, high conductivity (OFHC) copper for conductive pieces and Macor® glass* for insulative pieces. Both materials are easy to machine, and have excellent qualities for their roles and for maintaining an ultra high vacuum environment.

The simplest method for making the source removable is to build it in two parts. A removable assembly corresponding to the cathode of the MeVVA source allows us to pull the target sample back into the small chamber and replace an old target with a new one. Inside the trap a set of permanently affixed mounting rings provide a positioning mechanism and electrical connections. Cylindrical geometry allows us to keep the removable cathode in place without having to worry about its orientation with respect to the mounting rings.

The separate pieces for each part are designed to thread together removing the need for cements. The cylindrical geometry makes this design simple and effective. It is necessary, however, to machine the parts to high tolerances in order to ensure good electrical contact between the removable cathode assembly and the mounting rings. The source is designed to hold a cylindrical disk of boron carbide as the cathode target material. This target is held by compression when the cathode pieces are threaded together. By designing the source to have an interchangeable target, without the use of cements, we are able to use the same ion source for multiple experiments. In addition, we have the benefit of being able to replace the boron carbide disk with a similar sized disc of another conductive material. This ability allows the same source to be used in different plasma experiments.

Other of these issues require more significant deviations from typical MeVVA design. In a typical MeVVA source, a trigger arc discharges a high energy pulse

*Macor is a registered trademark of Corning Incorporated

to the surface of the cathode. As suggested by Ian G. Brown,[32] the creator of the MeVVA ion source, the trigger arc discharge alone may impart enough energy to the ions to reach the trapping region while remaining confineable. Thus, the source can be designed without a high energy discharge and without any extraction grids, relying solely on the trigger to keep the ions at confineable energies. In addition, the source is not intended to be used for ion beam systems or other high (or even low) duty cycle applications. One to a few shots should be sufficient for providing the number of atoms needed in the experiment, and so the source will not heat up significantly. Also, since we are working without the use of an extraction grid, the ion source operates at current densities well below the limit prescribed by Child and Langmuir in equation 1.1. The absence of heating issues allows us to remove cooling mechanisms, and simplifies the source design considerably.

Applying a mask to the source is simply done by using a 1/16" sheet of Macor between the target surface and the trigger electrode. The Macor has a small hole drilled in the region where the ^{7}Be spot lies on the target. This mask restricts the arc discharge to occur where the ^{7}Be is, but boron, carbon, and possibly also copper ions will also be produced. A mass–discriminator quadrupole field located in the trap is used to remove the boron, carbon, and other unwanted materials from the flow of ions while leaving only the beryllium to reach the trap.

There will inevitably be a small quantity of ^{7}Li present in the source as well, and the quadrupole field will allow that to pass through since its mass is similar to that of ^{7}Be. The design of the source is intended to minimize the time between creation of the ^{7}Be and its use in an experiment, thereby minimizing the amount of ^{7}Li from the start. A small quantity of initial ^{7}Li, however, will not be significant in the experiment.

Finally, the source is designed to allow relief to any small air pocket regions within

the source. Few of these exist in the source design. However, to keep low enough pressures to confine the plasma for a full half-life it is important to ensure the entire source can handle the ultra high vacuum pressures when inside the trap. The absence of air pockets also prevents internal arcs from occurring.

2.3 Insertion and Extraction Mechanism

The final aspect to discuss in this chapter is the means by which the source is removed from and inserted in the trap using only the axial motion of the manipulator arm. This aspect is, perhaps, the most difficult in this project to deal with, as the ultra high vacuum requirements restrict the methods employed. The mechanism needs to be simple, yet effective, while also not using much space inside the small chamber. Electrical connections would be possible, for an electrical switch type of mechanism, but would also be less desirable due to the difficulty of keeping wires from tangling or catching on protrusions and other pieces inside the trap while still being able to pull all of them back into the small chamber.

Though many possibilities were considered, the easiest mechanism seemed to be a piece that would flex down when inserted into a hole in the rear of the cathode assembly, then snap into place inside a groove cut on the inside of the cathode. This would allow the manipulator arm to push this extractor into the source, and keep the source attached to the extractor while pulling it back to the chamber. A set of grooves down the length of the inside of the cathode matching the fingers of the extractor allows us to remove the extractor from the cathode by rotating the piece by hand and sliding the fingers out along the grooves. (See Fig. 2.2.)

A second piece is used to insert the cathode assembly, consisting simply of a rod that fits the hole cut into the cathode base. This piece is designed only to support

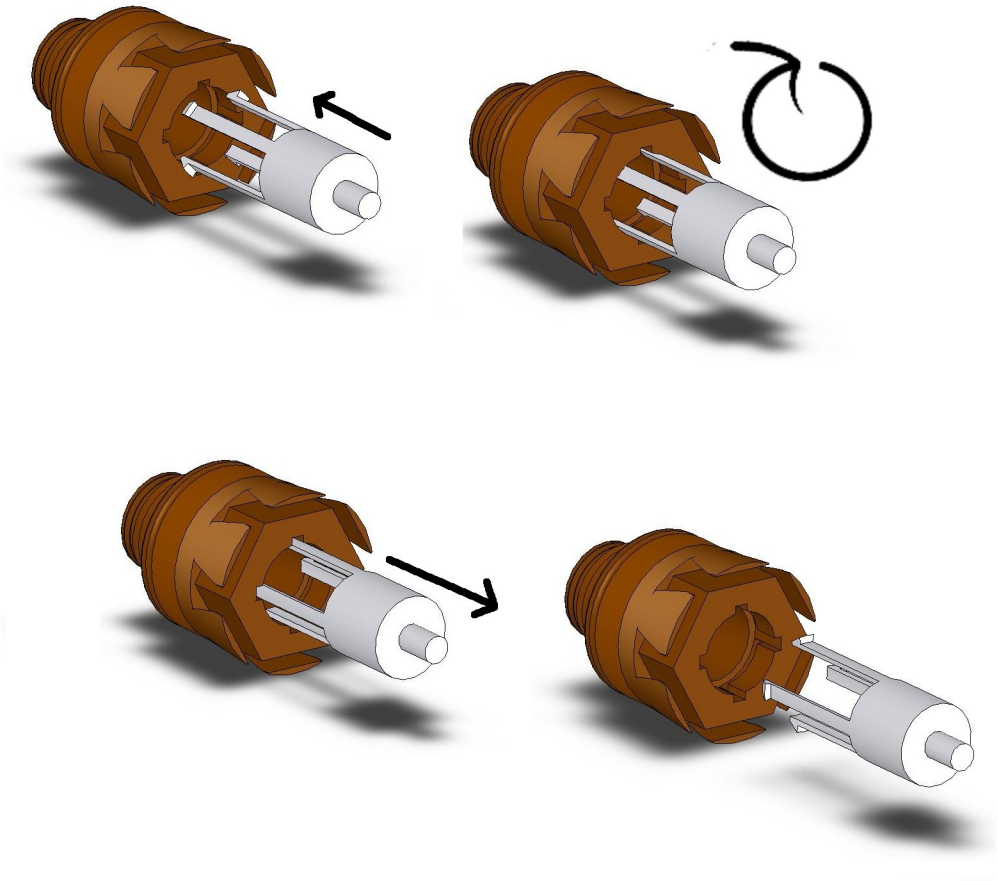

Figure 2.2 Schematic of the extraction mechanism.

the cathode assembly, and easily slides out when the cathode is in place. The two pieces must be stored inside the small chamber when not being used, to prevent contamination with materials that could affect the vacuum pressures inside the trap assembly.

These solutions address the requirements of the project, and provide a relatively simple design that is easily implemented. The following chapter will provide the details of the design and describe how all the pieces work together in the use of this ion source.

Chapter 3

Design of the source

3.1 Trigger

The initial component for the ion source design is a triggering mechanism to start the high voltage arc discharge on the cathode surface. This system consists of a simple 5 V pulse sent by a push button switch to a fast, high-voltage switch that sends a high voltage pulse through a step-up pulse transformer. The high voltage pulse from the transformer triggers an air spark gap to discharge a high voltage capacitor through a step-up transformer to the ion source. (See Figure 3.1.)

3.1.1 Pulse Transformer

The trigger circuit and pulse amplifier used is surplus from the Topolotron project done at Brigham Young University years ago. (See Fig. 3.2.) Some slight modifications were made, replacing a light-activated silicon controlled rectifier (SCR) with a regular SCR. The SCR discharges 1 kV provided by a 4 kV variable power supply through a high-voltage, high-current switch into a pulse transformer, yielding an 18 kV, 0.5 μs, low current arc in its output.

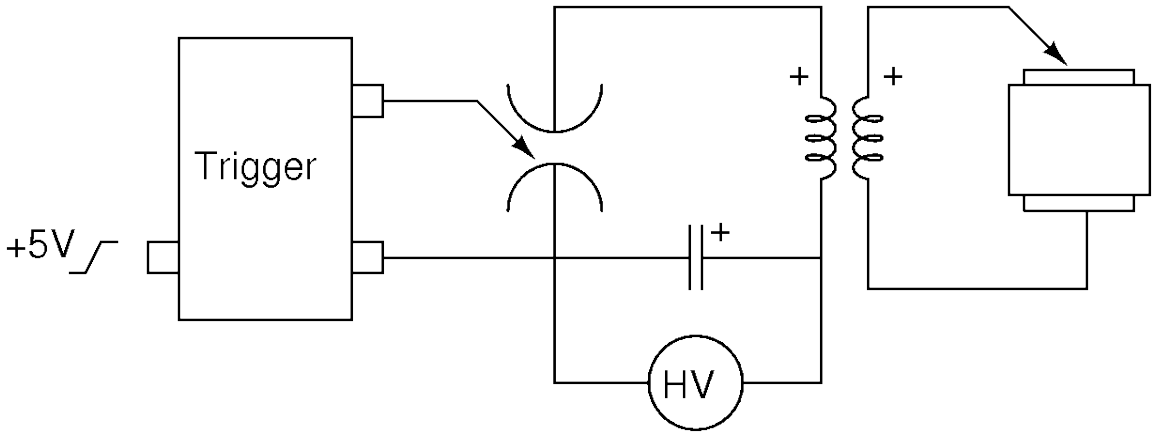

Figure 3.1 A basic schematic describing the trigger circuit. A more detailed set of diagrams can be found in Appendix B.

The pulse transformer was also modified to use a 20 V AC wall outlet transformer, rather than the 30 V alkaline batteries included when the transformer box was built. The ac input passes through a half-wave rectifier to power the SCR properly. The SCR is triggered with a simple 5 V pulse provided externally. For testing purposes, we used a monostable multivibrator and a push button switch to provide the 5 V pulse. In the actual experiment, an automated pulse system can be developed with a computer and easily implemented with the same results.

Other details about the pulse transformer, including a circuit diagram, can be found in Appendix B.

3.1.2 Spark Gap

The spark gap is built with two spherical electrodes made from 0.75 in brass rod. The electrodes are mounted in a plexiglass box with steel 1/4-20 rod, using washers and nuts to keep the electrodes from moving. The design also allows us to adjust the gap width by turning the rods through tapped holes in the box walls. Grooves are cut through one side of the box as a pressure relief for the air discharges.

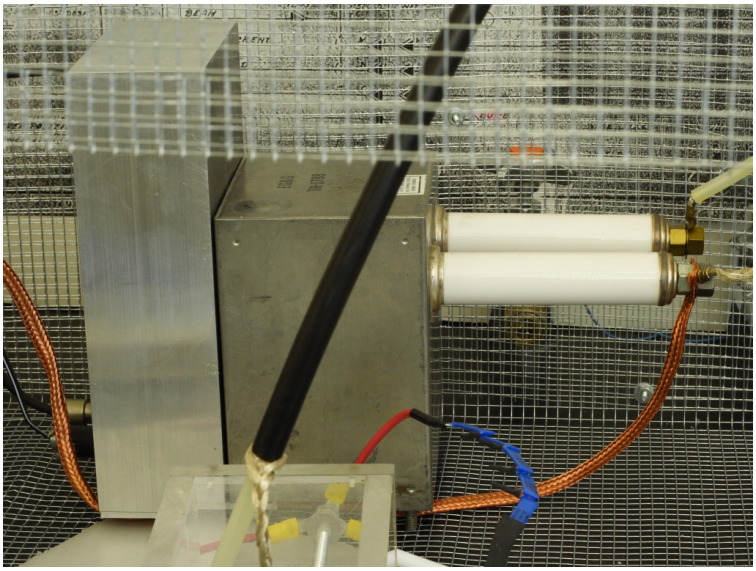

Figure 3.2 The pulse transformer.

The trigger electrode for the spark gap is simply a steel sewing needle soldered to a length of 12 gauge copper wire bolted to the box. The tip of the needle is bent inward slightly to discourage arcs from occurring in the direction opposite the current in the spark gap discharge. In spite of the high voltage in this trigger arc, the point of the needle has shown no sign of significant erosion, and so will remain an effective trigger mechanism for the experiment.

3.1.3 Capacitor Discharge

The primary arc discharge is accomplished using a 0.22 μF capacitor charged to a few kV using a 13.5 kV DC power supply and a Variac. The actual voltage applied to the capacitor is measured with a voltmeter at a voltage divider using a 1 GΩ and a 1 MΩ resistor. A high power 13 MΩ resistor in series limits the current while charging the capacitor. (This resistor is actually 4 separate 5 W 13 MΩ resistors, with two pairs of parallel resistors in series. The added power dissipation ability from

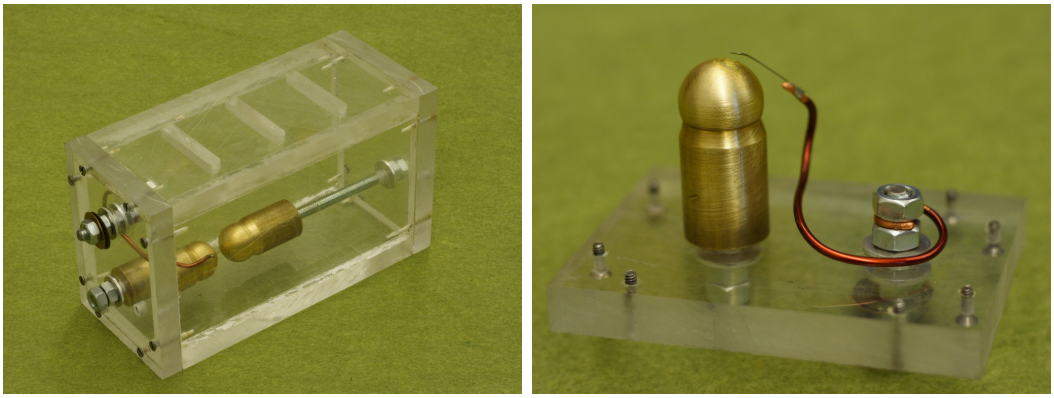

Figure 3.3 The air spark gap assembly used for the ion source, and a close view of the spark gap trigger electrode.

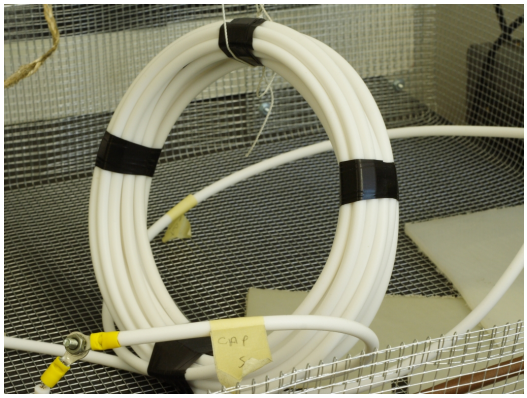

Figure 3.4 Step-up transformer used to transfer voltage to the ion source.

this configuration prevents the circuit from overheating.) The discharge is transfered to the ion source with a step-up transformer made from 10 gauge wire insulated with a thick (0.29" o.d.) teflon insulation. (See Fig. 3.4. This wire is actually M17/127 RGS-393 coax with the braided shielding removed.) The transformer has a 5:10 turn ratio to increase the voltage applied to the ion source. An air core is used, resulting in a little less than a factor of two increase in voltage.

The entire trigger circuit, except for the capacitor (due to its size), is enclosed in a well grounded Faraday cage to minimize noise and provide some degree of protection

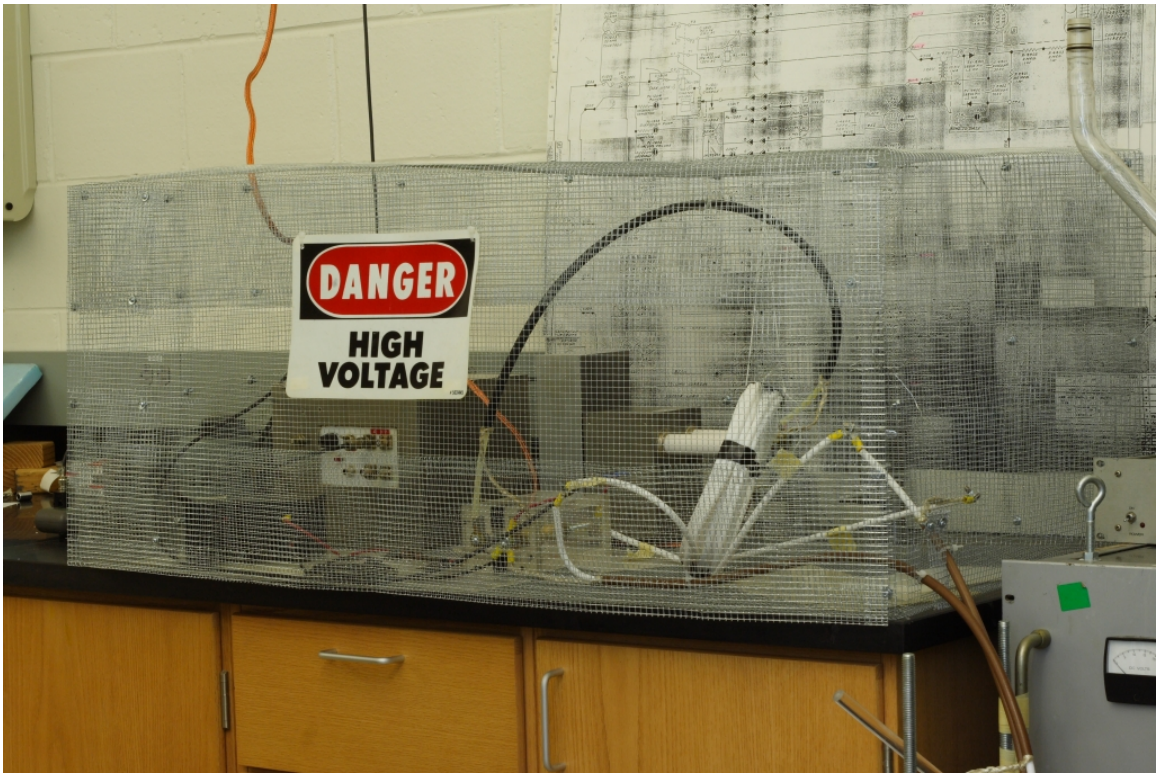

Figure 3.5 The entire trigger system enclosed in the Faraday cage for testing. This is not the same system that will be used in the actual experiment.

from the high voltages and RF radiation. (See Fig. 3.5.) Because the ion source is isolated from the trigger circuit, we are free to apply a voltage bias to the cathode rather than grounding it. The bias will be shown to improve the output of the ion source by minimizing released electrons without significantly increasing the energy of the ions. The bias is supplied with a separate, 100 V power supply.

3.2 Cathode Assembly

As mentioned in the previous chapter, the ion source itself is designed in two major parts: a removable cathode that includes the ^{7}Be target sample, and a set of mounting rings fixed inside the trap where electrical connections are made. Both use cylindrical

geometry, yielding a relatively simple design.

The boron carbide targets used in creating the ^{7}Be in our lab are disks just under 7/8" in diameter and 1/8" in thickness. There is a negligible amount of variation in the sizes of these disks. Much of the cathode design was based on the size of these targets. The cathode assembly itself consists of six pieces: a copper cathode base, the target itself, a Macor mask, a Macor locking ring, a copper trigger disk, and a copper cathode cap. (See Figure 3.6.*) The cathode base has an overall length of 2.3 in and diameter of 1.5 in (1.625 in at the end of the taper). It has a mass of 368 g.

The mechanism behind the source is simple: a high voltage is applied to the trigger ring, which arcs to the cathode base through the conductive target. The arc is a surface discharge along the inside face of the hole in the Macor mask. In order to get the discharge to occur in vacuum conditions, graphite is applied to this face to slightly increase its conductivity. The Macor locking ring holds the mask and the target firmly to the base, while the cathode cap holds the trigger disk firmly in place, lined up with the Macor mask, ensuring good electrical contact between the cap and the disk.

3.2.1 The Cathode Base

The cathode base is made from OFHC copper, and is roughly 2 inches in length and 1.5 inches in diameter. The back end of the base is slightly tapered to help the source line up properly with the mounting rings on insertion, and to help the electrical contact. Slits are cut into the taper to allow the copper to flex just slightly, helping hold the cathode in place when inside the trap. The front end is tapered down to the diameter of the target, and threaded to match the Macor locking ring. A groove near the middle provides a mechanism to lock the assembly into position in

*Machining drawings for all parts are found in Appendix A.

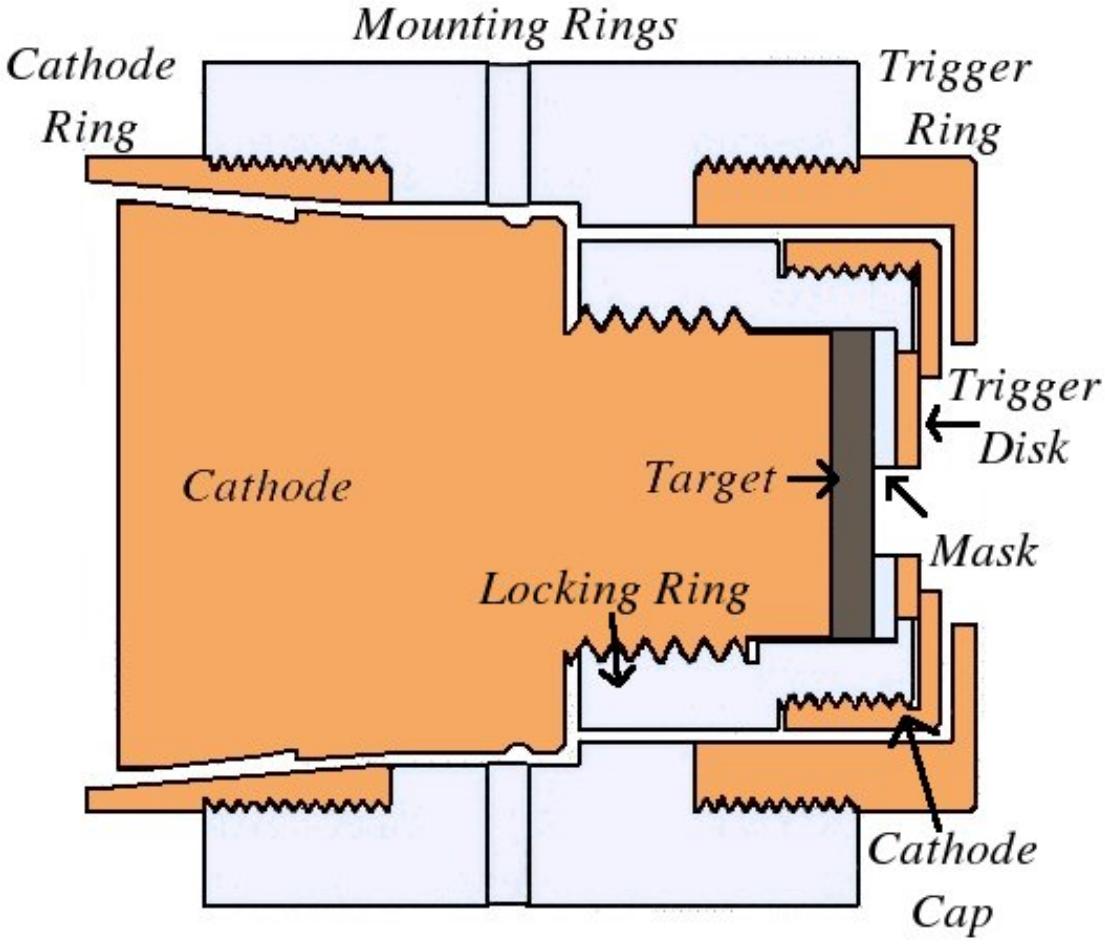

Figure 3.6 Schematic of the ion source assembly. Materials are color–coded, with the lightest color as Macor, the mid–tone as copper, and the dark shade as boron carbide. Not pictured is the interior of the cathode base, hollowed out and grooved to accommodate insertion and removal from the trap.

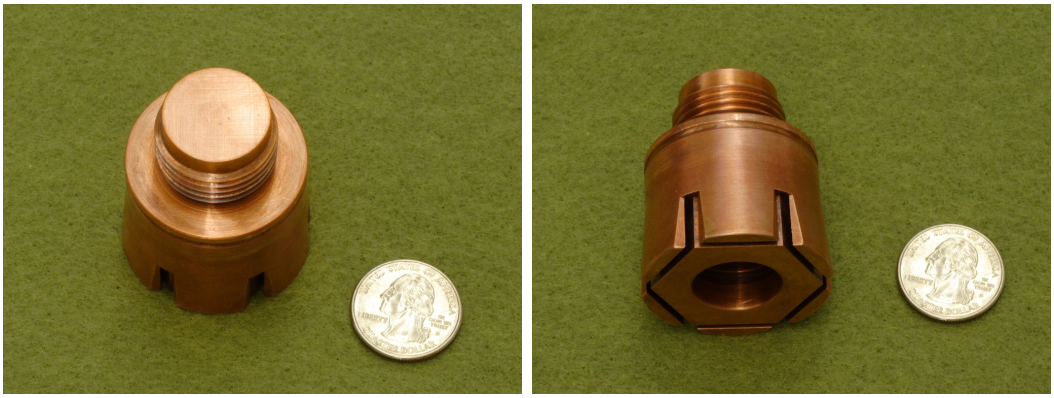

Figure 3.7 The cathode base.

the mounting rings by the use of spring loaded ball bearings. This mechanism will be further explained in the details of the mounting rings.

The inside of the cathode base is drilled out, partly to reduce the weight of the source, but also to provide a means of attaching the base to the manipulator arm. A rod attached to the manipulator arm slides into the hole to support the base, and pushes the assembly into the trap while easily sliding out to leave the source mounted in the rings. A groove is cut part way into the hole to allow the extractor to lock onto the base and pull the source out of the mounting rings on removal. A set of slits down the length of the hole match the arms of the extractor to facilitate its removal from the source.

3.2.2 The Locking Ring

The locking ring is a piece of Macor tapped to match the thread on the cathode base. The front end of the ring is threaded to match the trigger ring. A small lip overlaps the front edge to hold the target and Macor mask in place and to lengthen potential arc paths from the trigger to the cathode base directly. The lip is made thick enough to prevent cracking the Macor when the pieces are tightened, but thin enough to

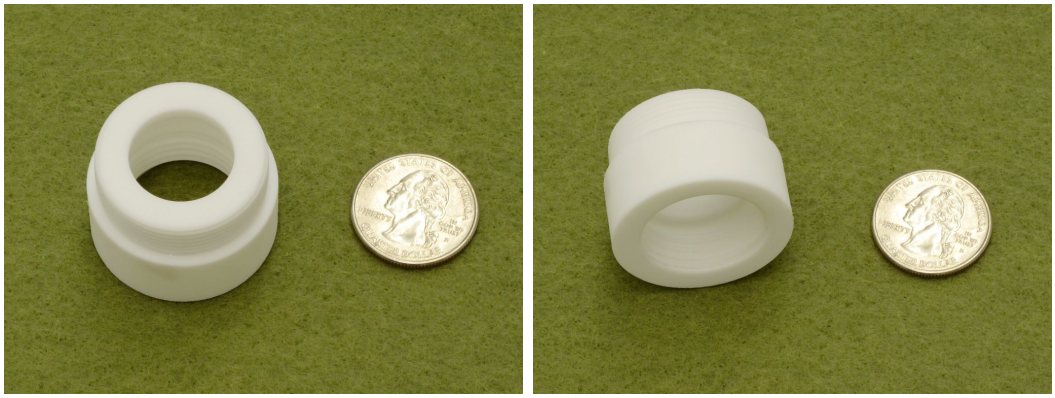

Figure 3.8 The locking ring.

Figure 3.9 The boron-carbide target. This target shows signs of use in the ion source, but has no ^{7}Be in it.

provide arc paths short enough for reasonable voltages. The ring is also cut short enough to not end up flush with the cathode base, ensuring the ring tightens on the mask and target rather than the cathode base.

3.2.3 The Target, Mask, and Trigger

The Macor mask is cut the same diameter of the target and has a small hole drilled into it to match the spot of ^{7}Be on the target surface. The trigger disk, made from

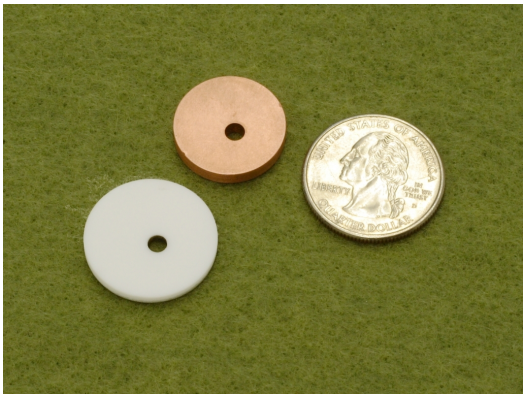

Figure 3.10 The Macor mask and trigger disk.

OFHC copper, matches the Macor mask, but has a slightly smaller diameter and larger thickness. This allows the locking ring to hold the target and mask in place but have the front end of the trigger disk extend beyond the locking ring. The protrusion of the trigger disk ensures the cathode cap will tighten on the copper, rather than the Macor, giving better electrical contact and reducing the risk of breaking the Macor.

It is important to note that the protrusion is very slight, minimizing the potential pocket of air between the trigger and locking rings. Slits in the threads of the rings provide pressure relief for the small air pockets present in this part of the source. Also note that all contact surface must be kept clean to prevent lower resistance paths on other surfaces. Oils from hands or other places can cause arcs to occur inside the source, between Macor pieces, or elsewhere rather than on the path between the trigger mask and the target surface. All of the pieces in the ion source clean very nicely with detergent and good scrubbing, followed by an alcohol wash to remove water condensation.

Figure 3.11 The cathode cap.

3.2.4 The Cathode Cap

The cathode cap is also made from OFHC copper, and is tapped to match the threads on the Macor ring. This ring is also cut short enough to not end flush with the locking ring. A lip on the front holds the trigger disk in place firmly, and with good electrical contact. The front of the cap butts up against the front end of the mounting rings. As this surface is that which makes electrical contact for the trigger, the face of the ring is cut with a very smooth finish to obtain good contact.

A final note regarding the cathode cap design is that the edge of the cap is filleted to help in the event the ion source is slightly off center. This situation could occur in spite of careful alignment of the mounting rings, since the weight of the cathode assembly may cause the manipulator arm to droop slightly when fully extended. The rounded edge will help lift the source when it reaches the edge of the mounting rings and put the source into its correct alignment without a great deal of force.

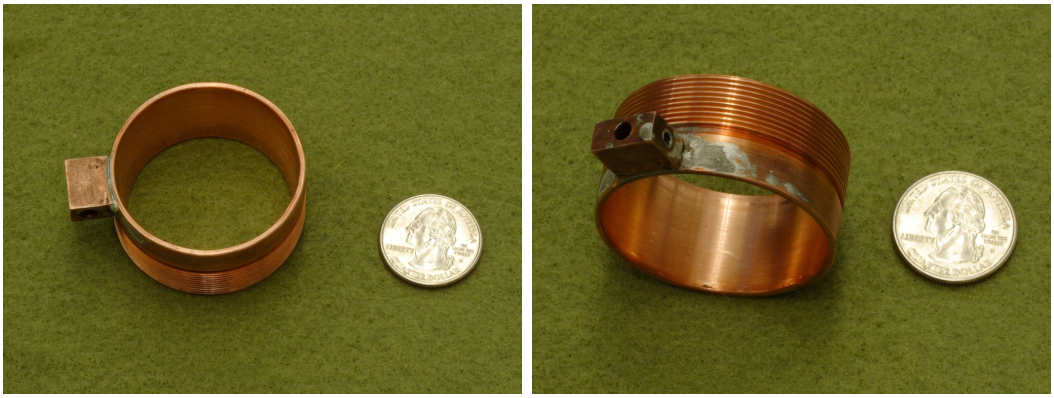

Figure 3.12 The cathode mounting ring.

3.3 Mounting Rings

The mounting rings consist of only three pieces: the cathode ring, Macor ring, and trigger ring. There is, in addition, a mounting bracket that holds the mounting rings securely inside the trap itself. The overall size of the ion source is determined by the size of these rings, resulting in a length of 2.375 in and a diameter of 2.25 in. These dimensions fit nicely into the trap with a minimum inner diameter of 4 inches while leaving enough space to prevent arc discharges between the trigger and the grounded trap wall. The mounting rings have a mass of 307 g, for a total source mass of 675 g.

3.3.1 The Cathode Mounting Ring

The cathode ring is also made from OFHC copper, with a taper that matches the taper of the cathode base. These tapers are machined with high tolerances to ensure there is good electrical contact between the cathode base and the mounting ring. The front end of the ring is threaded to match the Macor ring.

A small copper piece cut to match the curve of the ring is soldered to the outside of the ring. This piece includes a hole and set screw to mount a piece of ultra high vac-

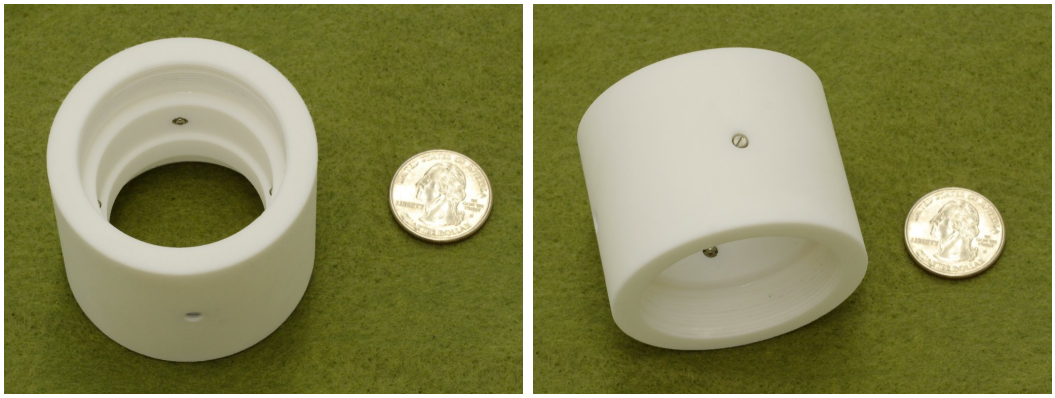

Figure 3.13 The Macor mounting ring.

uum compatible 12 gauge copper wire as an electrical connection to the feedthroughs where the trigger system is connected to the trap. Care was taken when soldering this piece to the ring to prevent damaging the precisely machined surfaces.

3.3.2 The Macor Mounting Ring

The Macor ring is cut with a wider diameter than the copper rings, with a good amount of overlap. These dimensions give a wide area to attach the mounting bracket and prevent discharges between the trigger and the bracket. Both ends are tapped to match the threads of the two copper rings, and a length of Macor in the middle with a smaller inner diameter insulates the mounting rings from each other.

Four holes are drilled and tapped in the back end of the Macor ring for a set of non-magnetic stainless steel spring-loaded ball bearings. These are aligned with the groove cut in the side of the cathode base. These bearings allow us to push the cathode assembly into the source, and snap into place when the cathode has reached its correct position. They also provide some assurance the cathode will remain inside the source when retracting the manipulator arm during source insertion. These holes are also slit to provide pressure relief.

Figure 3.14 The trigger mounting ring.

3.3.3 The Trigger Ring

The final piece in the set of mounting rings is another OFHC copper ring, threaded to match the tapped front end of the Macor ring. Note there is a difference between the threads on either end of the mounting rings because there is a correct direction for the rings to be mounted. This ring also has a copper piece similar to that on the cathode ring for electrical connection. The major difference in this ring is the front face, which has a hole wide enough to allow the ions through the source, but provides a face for the cathode to butt up against when inserted correctly. Again, this face is smooth to give good electrical connection.

3.3.4 The Mounting Bracket

The mounting bracket is a simple design, using two pieces. A curve in the center of each cradles the mounting rings firmly, and the pieces are bolted together to support them. Four arms (two on each piece) extend to the walls, where a set screw is tightened to keep the mounting rings from moving inside the trap.

Electrical connections are made to a high voltage feedthrough on the side of the

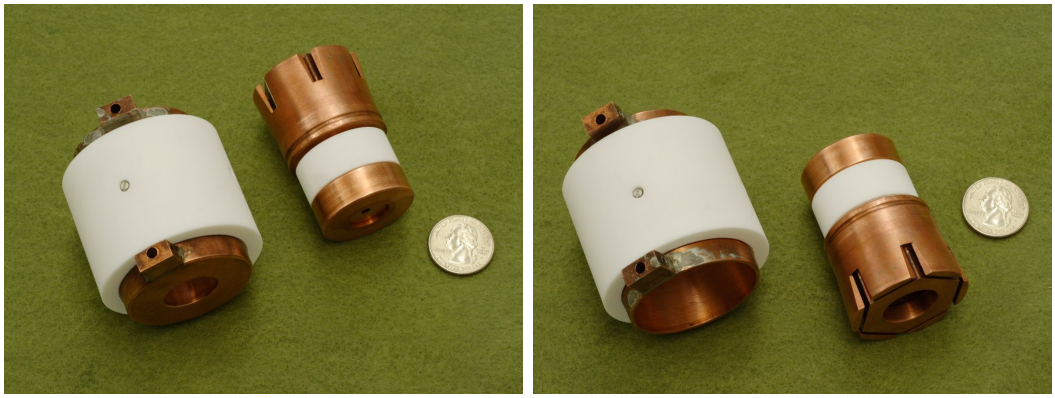

Figure 3.15 The assembled ion source and mounting rings.

trap wall. Bare copper wire is used to avoid vacuum issues with wire insulation, and so care is taken to ensure there is no contact between the wires and the mounting bracket or trap wall.

3.4 Insertion and Removal Mechanism

The attachments to the manipulator arm for working with the ion source are both made from 1 inch aluminum rod. The manipulator arm is built with a 1/4-28 tapped hole, so both pieces are designed with a corresponding threaded end for attaching to the arm. Both pieces have a length of 2 3/8", which leaves room in the opening to the small chamber for both the attachments and the source when connected.

The insertion attachment is simply a rod, with the leading end turned down to match the hole cut into the back end of the cathode base. The fit between the two is close enough to give good support to the mass of the cathode assembly when the arm is extended, but loose enough to not stick when the cathode is in place. This piece is stored inside the small chamber, out of the way of the arm, to prevent contamination with materials that might affect the vacuum conditions inside the trap.

The extractor attachment is more complicated, with a set of fingers that extend from the base to secure the cathode assembly (See Fig. 2.2 and the machining chart on page 74). These fingers are approximately 1/16 inch thick and 1/8 inch wide to be sturdy, yet flexible. The ends extend up to snap into the groove, with the front end chamfered to help the fingers bend downward when in contact with the back end of the cathode. There are four fingers total, spaced equally around the circumference. The extractor is removed from the cathode by rotating the fingers in the groove inside the cathode base until the fingers line up with the slits down the base, allowing easy removal without having to flex the fingers by hand. This attachment is also stored inside the small chamber when not in use.

Chapter 4

Source testing

4.1 Testing Environment

The ion source was tested inside a vacuum bell jar at our laboratory (Fig. 4.1). During the experiment, the source will be in a horizontal configuration with respect to the trap. For convenience, however, testing was done with the source held vertically. The ion velocities coming from the ion source are high enough that gravitational effects are negligible, so the behavior of the flow of ions is approximately the same in either configuration. The source was placed under a grounded copper plate and shielded with copper mesh to prevent large noise signals appearing in the measurements by pickup in the cables (Fig. 4.2).

Most of the measurements were taken with a copper Faraday cup. The cup is held above the source and catches ions flowing away from the cathode. The ions deposit a charge on the cup that can be measured. Energy transferred to the cup by the ions can result in emission of electrons from the copper, as its work function is only 5 eV. The length of the cup was designed to recollect these secondary electron emissions and reduce the error on our measurements.

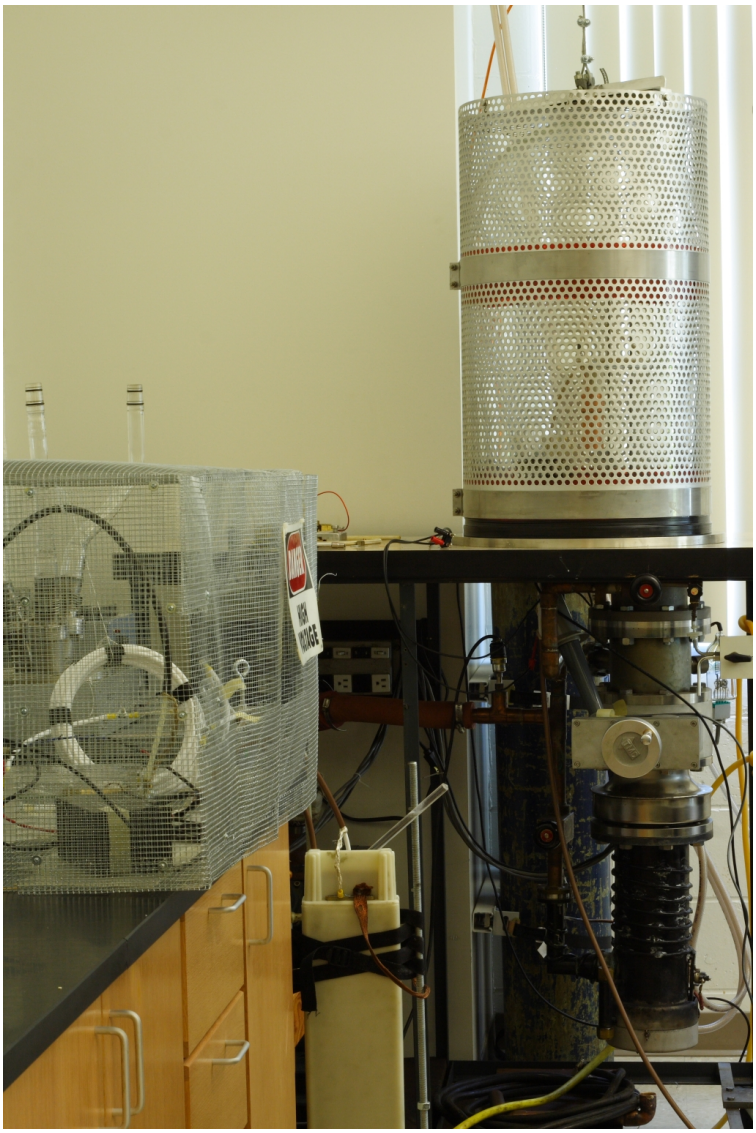

Figure 4.1 The vacuum bell jar used for testing. Also seen are the trigger inside a Faraday cage and the high-voltage capacitor used in the discharge.

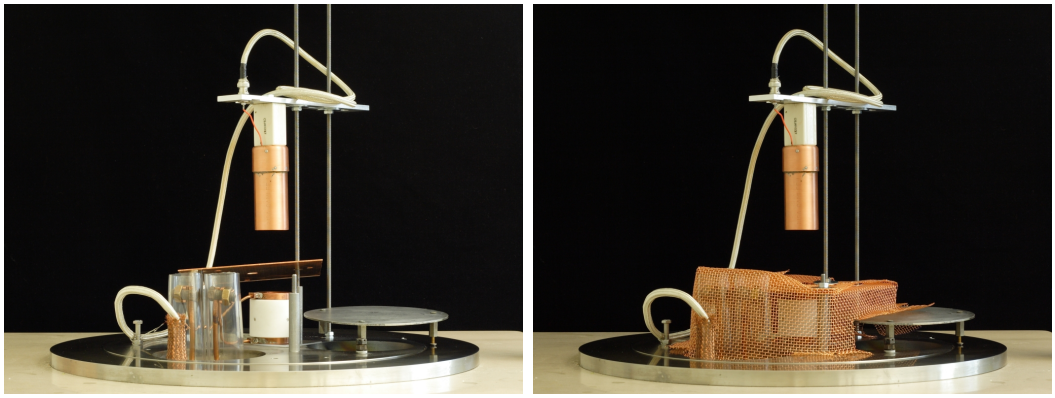

Figure 4.2 The ion source is mounted inside a vacuum bell jar in the vertical position. A grounded copper plate and copper mesh shielding provide a Faraday cage inside the jar. The Faraday cup is held above the ion source.

The cathode is insulated from the base of the bell jar, and can be biased to a positive voltage to minimize electrons released by the source in the flow, and to help the ions leave the source more directly. A passive integrating circuit is attached to the Faraday cup to analyze the received signal from charges hitting the cup (See Appendix C).

The integrated signal was measured with a digital oscilloscope. A separate digital oscilloscope was used to monitor the arc discharge. Both oscilloscopes also monitored the trigger signal to ensure proper alignment of timing when comparing the signals.

For testing purposes, we charged the capacitor to 4 kV, resulting in about a 7 kV initial arc on the source. The spark gap was adjusted to be wide enough to prevent breakdown at that voltage, but small enough that the presence of the trigger arc consistently allowed breakdown. Pressures inside the bell jar were typically 6 μTorr. This pressure is much higher than the pressure inside the ultra high vacuum of the trap, but is still low enough that neutral collisions during the time scales of firing the source are negligible. The bias of the cathode and distance between the source and the Faraday cup were varied for analysis.

4.2 Source Behavior

Numerous tests were performed to understand the characteristics of the ion source and to prove its ability in creating a ^{7}Be ion plasma.

4.2.1 Faraday cup signal

Figure 4.3 shows a typical measurement taken with the Faraday cup using this system. This data was taken with the cup held 25 cm from the source and a 100 V bias applied to the cathode. A small noise signal from the arc discharge occurs at 10 μs after the initial trigger. This noise tells us there is a 10 μs delay between triggering the spark gap and triggering the vacuum arc to the ion source.

A clear signal implying collected charge appears roughly 10 μs after the discharge, giving us a rough estimate of the ion velocity at about 25 km/s, a speed typical of MeVVA sources.[32] The dips in the signal are attributed to pulsing in the arc discharge of the ion source. The voltage applied to the source is seen to oscillate, and an arc occurs every time the voltage gets high enough to cause breakdown. Each arc causes a burst of ions to be released and hit the cup. The signal is seen to decay by normal RC discharging of the integrating capacitor through the passive integrator circuit resistance. The amplitude of the signal can be used as a measure of the number of charges coming from the ion source.

4.2.2 UV photo-electron emission vs. actual ion emission

Because of the low work function of copper, we must consider that the signal could be produced by UV light in the 5–10 eV range. To ensure this signal is caused by charge collection and not photo–electron emission from the cup due to UV radiation from the arc discharge, the signal was analyzed with a sapphire window between the source and

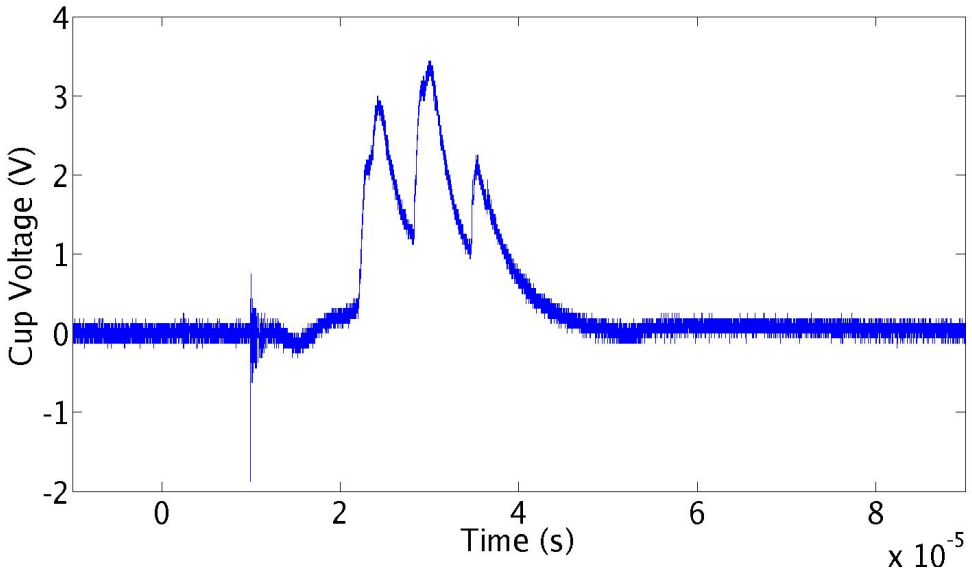

Figure 4.3 Typical integrated signal from the Faraday cup, measured 25 cm from the source with a 100 V bias applied to the cathode.

the cup to allow only the optical signal to pass through. The measured signal from the Faraday cup in this test matched the noise signal obtained on oscilloscope channels not even connected to the circuit (Fig. 4.4). The lack of signal on the Faraday cup in this test clearly demonstrates that the source is indeed producing a stream of ions.

4.2.3 Arc Discharge

With a fused quartz window in place, we also examined the optical signal of the arc discharge using a photodiode. The measured signal shows oscillations corresponding with the oscillations in the arc voltage (Fig. 4.5). This test shows that each discharge actually consists of multiple arcs occurring on positive voltage swings in the oscillation of the capacitor discharge. After the arc is extinguished, the arc voltage shows the capacitor voltage still continues to oscillate at its natural frequency in the circuit as it discharges without enough energy to cause a vacuum arc in the ion source (Fig. 4.6).

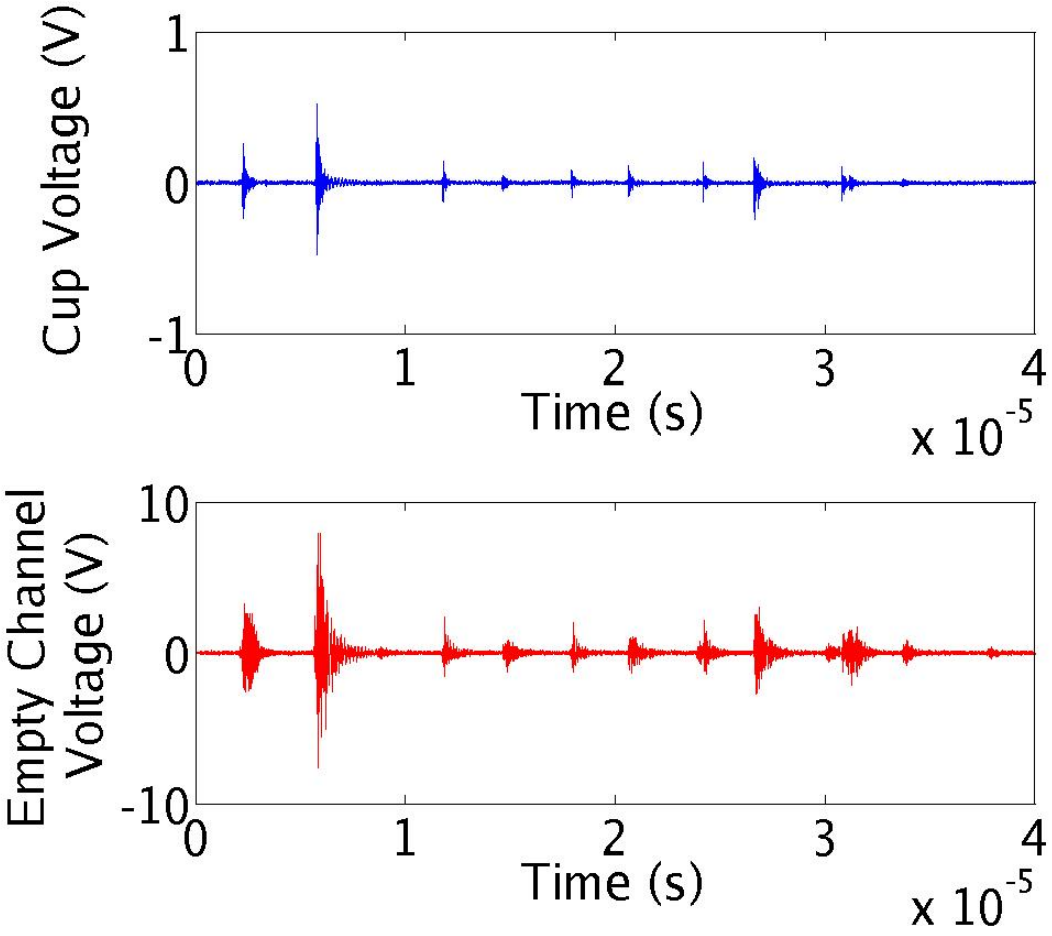

Figure 4.4 A comparison of the electrical signal on the cup with a sapphire window between the source and the cup to the electrical noise signal picked up on unused channels of the oscilloscope.

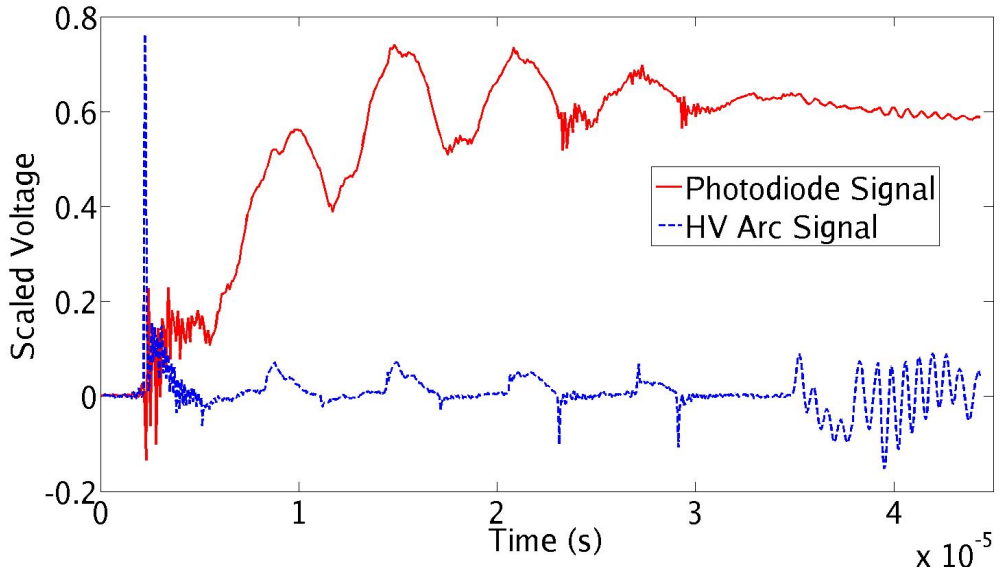

Figure 4.5 Measurement of light signal from the arc. Oscillations correspond to the oscillations in the high voltage signal from the discharge capacitor, implying multiple arcs are occurring in the source. In this graph, both plots are scaled for comparison.

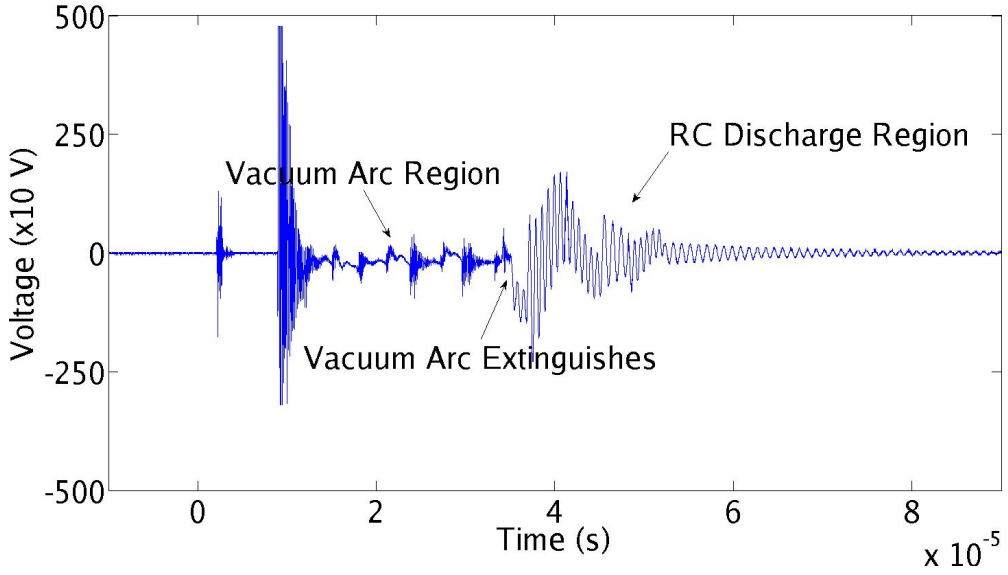

Figure 4.6 This graph describes the events in the lifetime of the vacuum arc as seen by the high voltage signal from the discharge capacitor.

4.2.4 Reproducibility

The signal obtained from repeated shots with the same applied voltages are quite reproducible, as seen by the overall shapes of the signals plotted in figure 4.7. Each plot has three peaks, corresponding to three major pulses of ions from the source. The timing of the three peaks is very similar between each shot, showing the ion flow has roughly the same energy from shot to shot. We do expect variation in the signals due to arcs originating from different cathode spots, but the overall variation is not significant.

After a series of 25 shots, we could, however, detect a decrease in amplitude, also seen by a decrease in visual intensity of the arc discharge (Fig. 4.8). This reduction is probably caused by a decrease in the conductivity of the inside surface of the Macor mask. As the source is used, ablated material will also deposit on the sides of the mask and trigger disk while the flow of ions expands outward. The boron released from the source will reduce the overall conductivity of the arc surface, yielding a weaker discharge.

4.2.5 Ion Velocity

An analysis of the result from adjusting the source–cup separation and the applied bias both show expected results for charges being released. We made measurements at 14 cm, 25 cm, and 40 cm. Further distances increased the signal's delay and decreased its amplitude (Fig. 4.9). We find that the signal is much stronger and occurs earlier when the cup is held closer to the source, and that the peaks attributed to bursts of ion emission from the cup are more pronounced. At the farthest distance, the peaks have smeared together almost completely, suggesting that the ions in the beam have a spread in velocities. The three pulses then mix together as the beam travels further

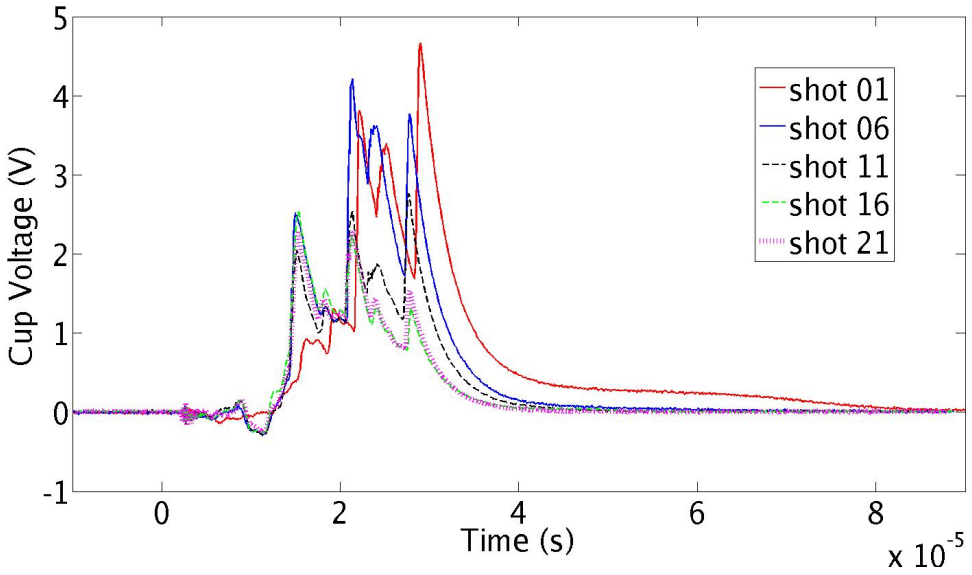

Figure 4.7 Similar voltage configurations result in similar signals obtained on the Faraday cup.

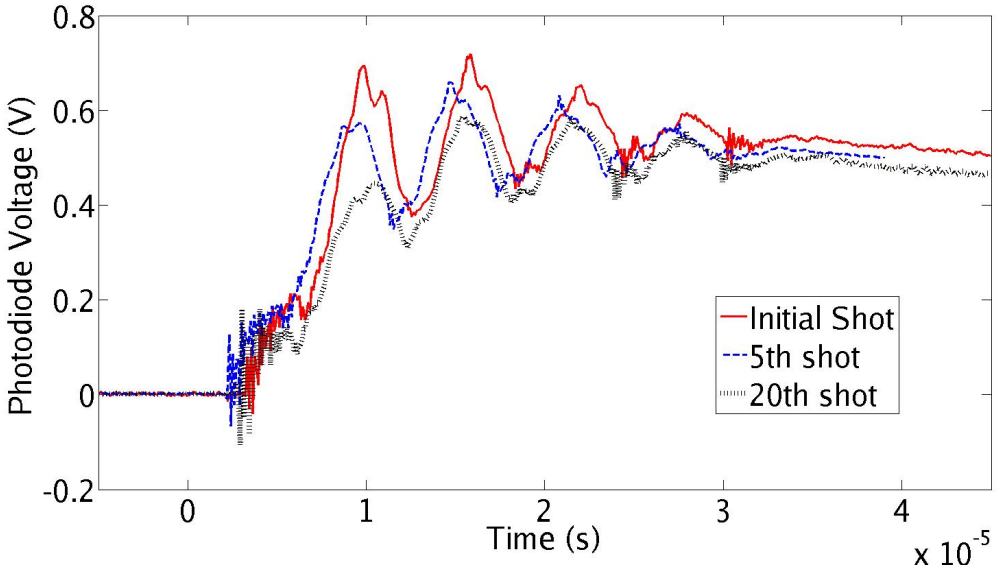

Figure 4.8 The visible light detected with a photodiode decreases in intensity as more shots are taken.

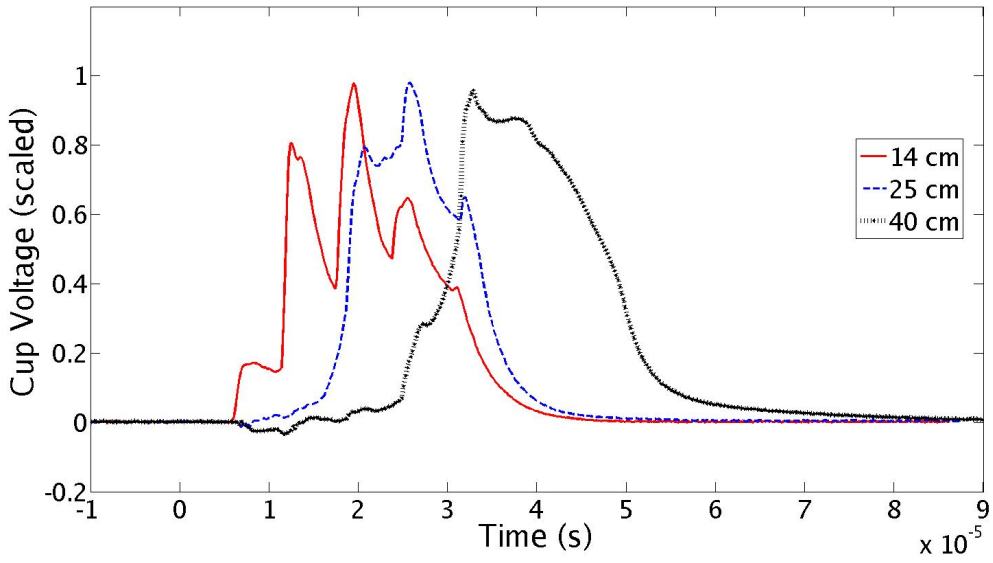

Figure 4.9 Moving the cup away from the source shows a delay in the signal. The amplitude decreases significantly with separation, so all signals are scaled to a range of -1 to 1. The 14 cm signal is scaled down by a factor of roughly 16.9, the 25 cm by a factor of 5.6, and the 40 cm by a factor of 1.6.

from the source.

Using the data to measure the time between the arc discharge and the charge build-up on the Faraday cup, we can get an estimate for the velocity and thermal energy of the ions coming from the source. The data from the 14 cm, 25 cm, and 40 cm cup distances in figure 4.9 show an ion velocity of 25.2 km/s, 25.7 km/s, and 22.9 km/s respectively. These values are all consistent with typical velocities measured by Brown et al.[32] Using these velocities, we find the ions have an energy between 15 and 25 eV. This energy is easily confineable with our trap.

4.2.6 Bias Voltage

Varying the bias shows a significant effect on the quality of the flow of ions, but little effect on the energy of the ions. We applied biases of 0 V, 50 V, and 100 V. A slight

increase in velocity is seen with higher bias voltage, though not enough to cause a concern for confinement. More importantly, at 0 V bias, the passive integrator detects a negative signal, corresponding to free electrons hitting the Faraday cup. These electrons would cause the cup to measure an overall low value of charge from the ion source. Applying a bias essentially removes the electrons from the flow, and allows us to make a more accurate estimate of the number of charges produced by the ion source.

In addition to removing electrons from the flow, the bias voltage also has a focusing effect on the ion flow. We expect an expansion in the flow of ions as they drift from the ion source and repel each other. The added bias appears to reduce the rate of expansion, allowing more charges to reach the Faraday cup at farther distances. This effect is seen in our data with a stronger signal at higher bias, in spite of little change in the actual energy of the ions. The beam profile is analyzed and discussed more fully in section 4.3.2.

4.3 Charge Output

The previous tests indicate that a substantial charge is released in each shot from the ion source. The passive integrator provides a means of determining how much charge is present in each shot. We can assume the charge state is not exceptionally high, a likely assumption given the energies of the ions determined previously and given the binding energies of the atoms present in the ion flow (see table 4.1). This measurement, then, corresponds to a good estimate for the actual number of ions released from the source.

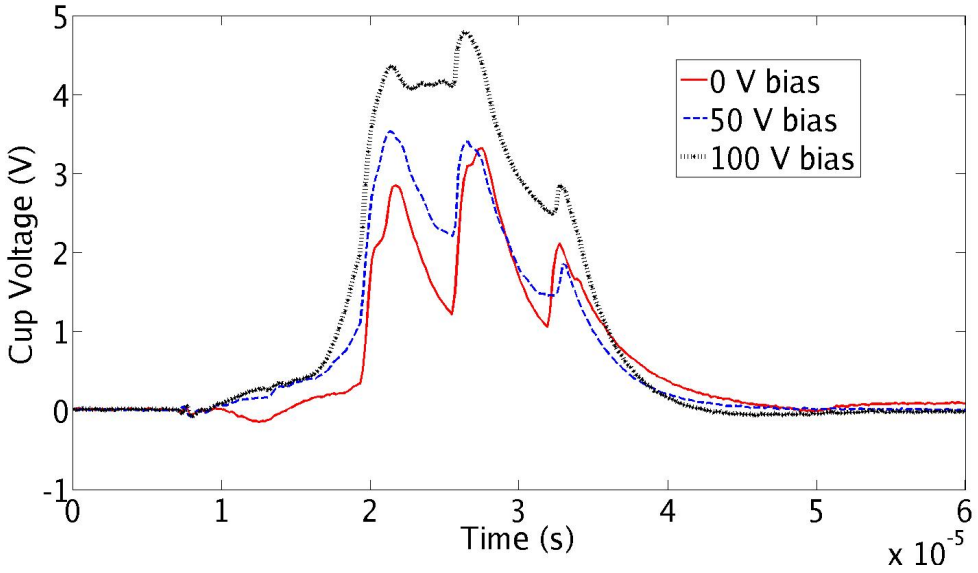

Figure 4.10 Increasing the voltage bias on the cathode shows a decrease in electrons and an increase in ions in the flow, marked by a stronger positive value in the integrated signal. A slight increase in velocity is also seen.

Ionization State:	I	II	III
Be	9.32 eV	18.2 eV	153.9 eV
B	8.30 eV	25.2 eV	37.9 eV
C	11.26 eV	24.4 eV	47.9 eV

Table 4.1 Electron binding energies of the three major components in the ion flow from the source. (^{7}Be is not, of course, present in the tests presented here.)

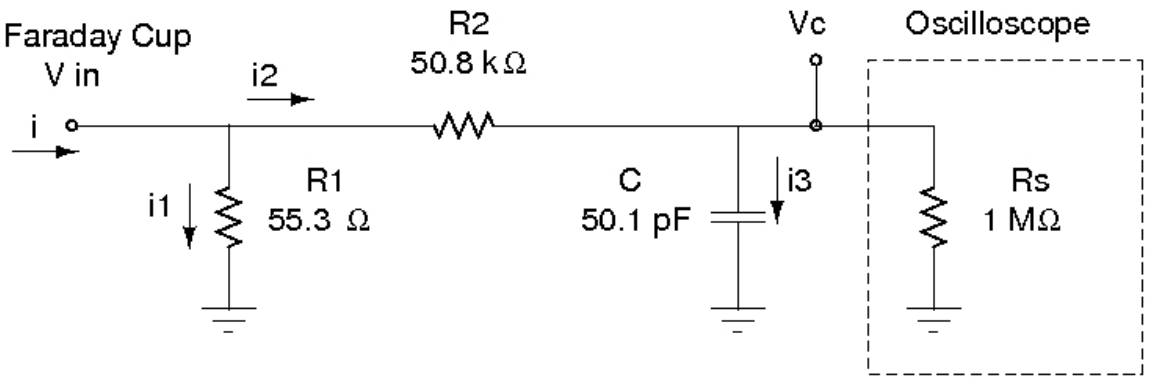

Figure 4.11 The passive integrator circuit.

4.3.1 Faraday Signal Integration

The integrator circuit (Fig. 4.11) is very simple, but the total current into the Faraday cup is not the same current that passes through the integrating capacitor. The integrator can, however, be analyzed using Kirchoff's loop rules to find a coupled set of Differential-Algebraic Equations (DAEs) that describe the behavior of the circuit given a current input. These equations can then be solved for the input current in terms of an algebraic expression relating the measured voltage (V_c) as well as the derivative of the measured voltage (V_c'). Other parameters involved in this calculation are the terminating resistor (R_1), the dividing resistor (R_2), the oscilloscope resistance (R_s), and the integrating capacitor (C):

$$i = \frac{R_1 + R_2 + R_s}{R_1 R_s}\, V_c \;+\; \frac{R_1 + R_2}{R_1}\, C\, V_c' \tag{4.1}$$

Because this equation requires the derivative of the measured data, averaging was used to smooth the data in making this calculation. It can be shown that the equation is robust enough that smoothing does not have a significant effect on the numerical value obtained (See Appendix D). Integrating the result over time yields the total charge passing into the circuit.

Using the dataset from 25 shots on a single boron carbide target, we find that

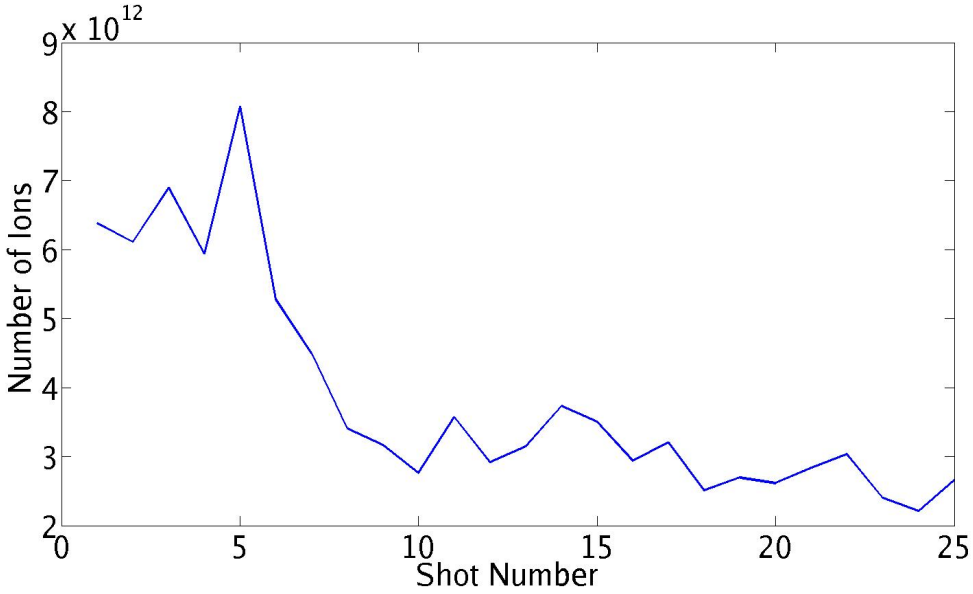

Figure 4.12 The number of ions released by the ion source plotted against the shot number. The plot shows that the initial discharges are slightly stronger until excess graphite has been blown off of the arc surface. The strength of the discharge continues to decrease gradually as the path length increases when more of the surface is ablated.

an average of 6.2×10^{-7} C of charge were collected by the Faraday cup at a distance of 25 cm. Assuming these are mostly singly ionized atoms, this corresponds to 3.8×10^{12} ions, more than sufficient for the needs of the experiment.

4.3.2 Beam Profile

Using the same technique for measuring the charge on the cup, we can compare the measurements at different distances to find an estimate on how rapidly the flow of ions is expanding. This analysis assumes that at 14 cm, the Faraday cup collects the entire charge, and that the density of the beam is inversely proportional to the radius of the beam. The radius of the beam at a given distance is then

$$r = 4.125\sqrt{\frac{Q_0}{Q}} \tag{4.2}$$

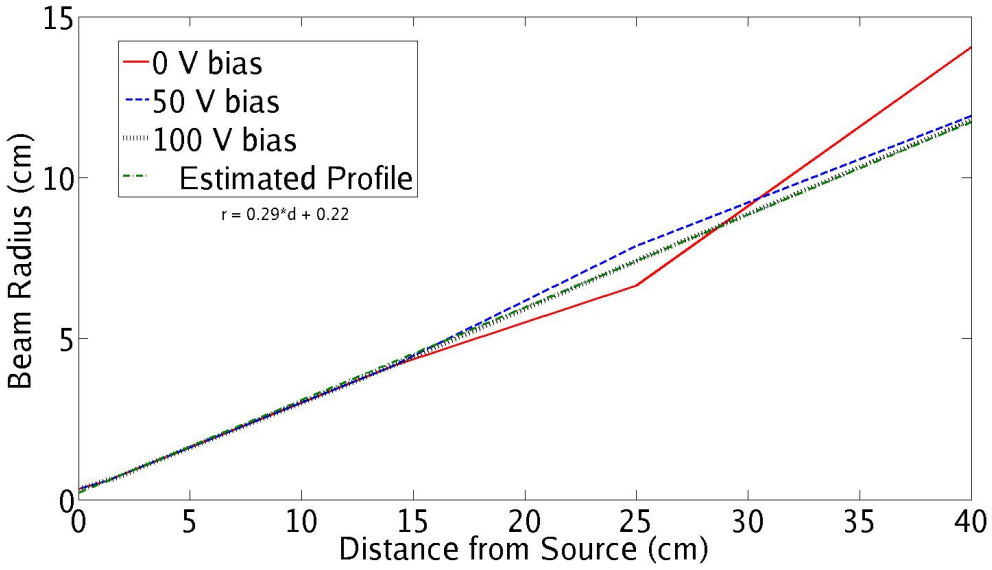

Figure 4.13 A description of the beam profile, or the rate of expansion for the flow of ions from the source.

where Q_0 refers to the total charge emitted (as measured at 14 cm) and we make use of the diameter of the Faraday cup (4.125 cm).

Figure 4.13 shows a typical comparison of the profiles at different bias voltages. This test is just for a general understanding of the flow expansion. Bias voltage seems to focus the flow of ions slightly, and an expected linear profile is plotted against the three sets of data. This data suggests that the beam expands by 3 cm every 10 cm away from the source. The wall of the trap begins 5 cm in radius from the center, and so we would expect the flow to reach approximately 12 to 15 cm down the trap before hitting the wall. This is farther than the ions will travel before entering the quadrupole, and so there is little concern for high ion loss to the walls of the trap; most of the ions will reach the region they need to.

It should be noted that this result is not completely consistent due to variability between shots, and data can be easily found that implies the 50 V bias actually has a narrower beam width than the 100 V bias. It seems that positively biasing the

cathode at all has a focusing effect on the beam, regardless of the magnitude of the bias. The 100 V bias does, however, have the added benefit of removing more electrons from the flow of charges.

4.4 Surface Behavior

4.4.1 SEM photography

In addition to the electrical testing, we have examined the surface of the target using a Scanning Electron Microscope (SEM) to see the effect of the arc discharge on the surface of a bare boron carbide target. Our sample was done with a clean target and 25 discharges. Figure 4.14 shows an image of the unmasked portion of the target. The primary discharge clearly occurs in one region, but surface ablation from secondary arcs occurred in places over the whole surface of the region, showing we can extract ^{7}Be from the entire unmasked region. In addition, these images suggest ablation to depths of up to 10 μm has occurred, far more than necessary as the ^{7}Be deposition on the target only extends a few microns into the surface (Fig. 4.15).

Closer examination of the target surface in the primary ablation region reveals the energy of the arc discharge was enough to melt the boron carbide (Fig. 4.16). As the material cooled, minute cracks formed just as would be expected in rapidly cooling materials. In addition, crystal formation can be seen near the cracked regions.

4.4.2 Optical Microscopy

The target surface was also examined with an optical microscope to gauge the depth of the ablation into the surface. Due to the size of the surface features (and to problems with the alignment of the CCD camera installed on the microscope), clear photographs

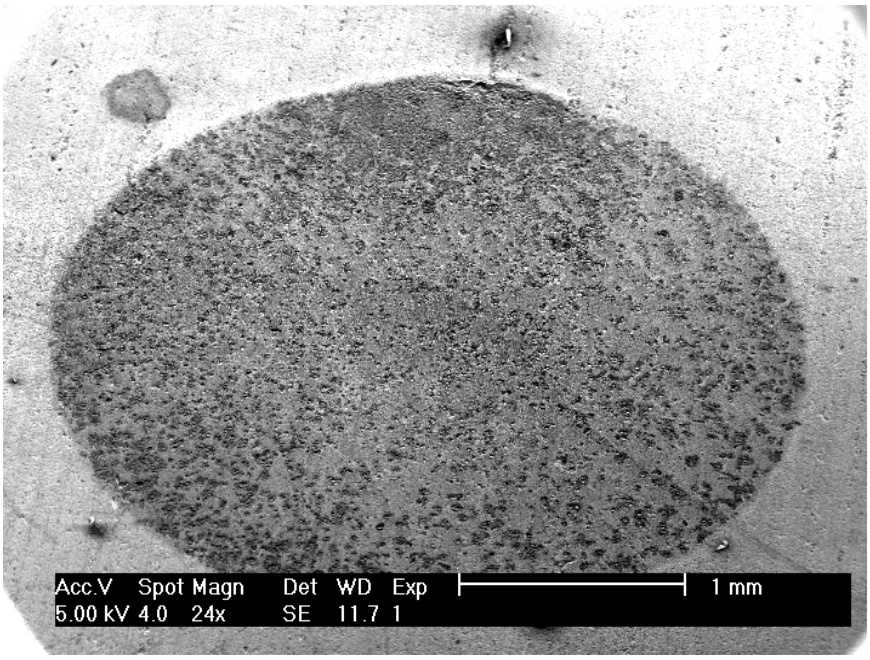

Figure 4.14 SEM photo of the unmasked region of the target surface.

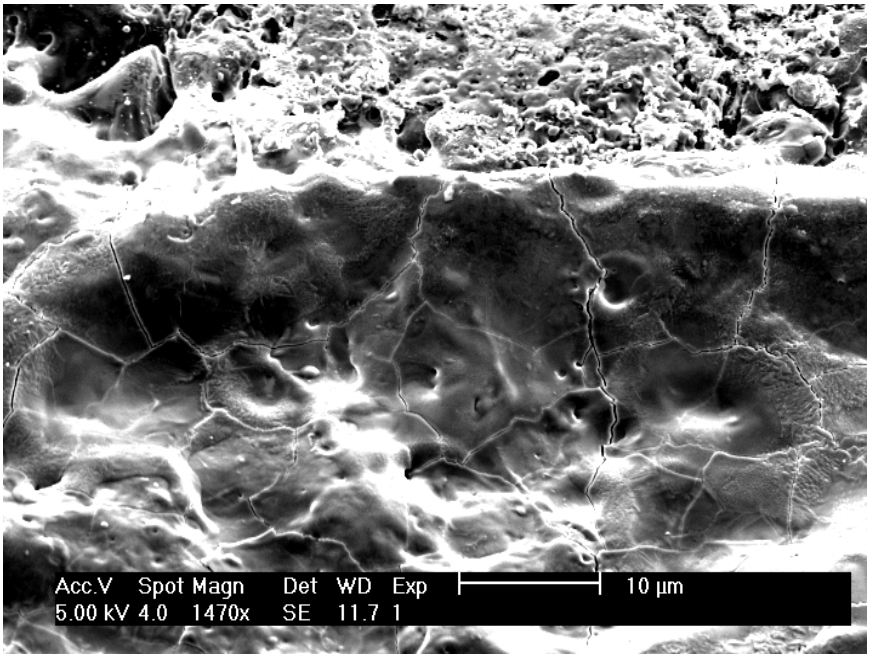

Figure 4.15 SEM photo showing the deepest ablation in the target. The scale of the photo suggests the depth of the ablation is as much as 10μm.

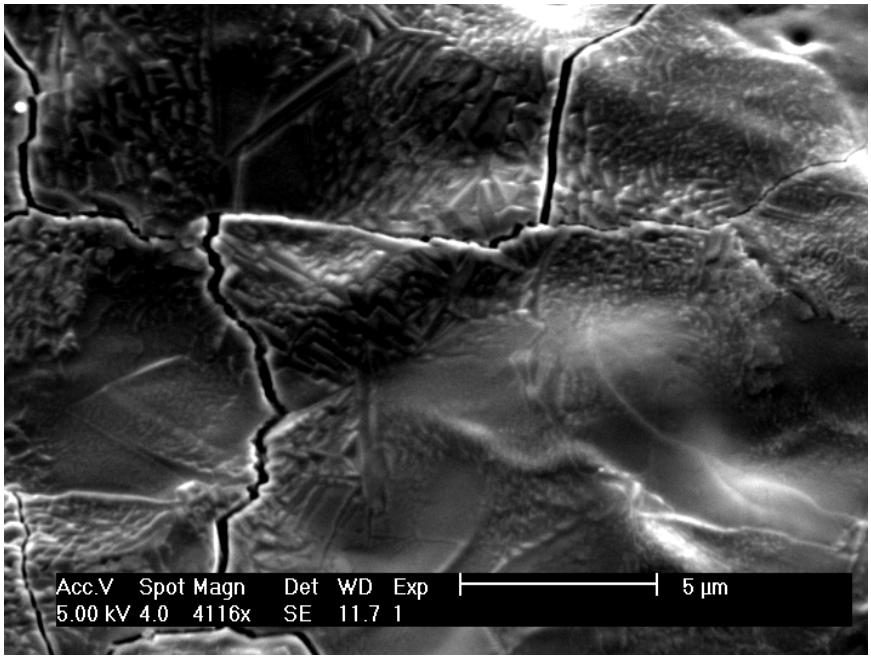

Figure 4.16 SEM photo of the primary ablation region, showing melting, fracturing, and crystal formation.

of this measurement at visible wavelengths are, unfortunately, unavailable. However, by focusing the microscope on the surface of the unablated target and then on the deeper parts of the ablation region, we were able to measure a depth of 8 microns at the edge, confirming our estimates made with the SEM photos. This measurement was achieved by noting the distance the objective of the microscope was moved between focusings.

Chapter 5

Discussion of Results

Though the required characteristics of a ^{7}Be ion source posed some difficult problems, the solutions have been surprisingly straight forward. The method of using a screw-together system to allow easy exchange of the target sample is quite simple, and yet rather elegant because of its easiness. It should be pointed out that one of the key factors in the success of this design was the selection of materials that turned out to be easy to use and well suited for their purpose. It is necessary, however, to treat those materials correctly to maintain their quality in this application. In particular, the Macor pieces need to be carefully handled and well cleaned as the ion source is maintained.

Inserting and removing the source is quite easy, and the design minimizes the complexity of the system to connect and disconnect from the electrical circuit. Care must be taken in installation to ensure the mounting rings are centered correctly, though small error can be compensated by the source's filleted edge to pull the cathode into alignment. That said, it would be difficult to insert the extractor to remove the cathode if it is too far out of alignment with the manipulator arm.

This design has provided us with a sturdy, well-built ion source that accommodates

all of the peculiar requirements of this study. The electrical connections have proved solid, and the ion source has proven to be effective and consistent.

5.1 Source Behavior

The extensive testing of this ion source gives us a good understanding of what to expect from it in use during an experiment. Vacuum arcs are easily obtained using only 4 kV (7 kV applied to the source) at a few μTorr. At lower pressures in the ultra high vacuum environment of the trap, we may be required to increase that voltage, though certainly not to any unreasonable value. The use of a Variac on the spark gap power supply makes this adjustment easy to do.

It is essential to have a thin coat of graphite on the inside of the Macor mask to initiate the vacuum arc, though it should not be applied too liberally. If the source is found to have weak discharges, it may be necessary to apply more graphite to the surface. The graphite is easily cleaned off when the Macor is thoroughly scrubbed, and will certainly need to be reapplied after pieces have been cleaned.

5.2 Charge Output

The testing also shows conclusively that the ion source is capable of producing a large number of charges with each shot. Because of the nature of the design, each shot will not only release ^{7}Be ions, but also boron, carbon, and perhaps copper ions as well. These are removed with the quadrupole section of the trap assembly, but given the number of ions produced a large number of ^{7}Be ions will reach the quadrupole fields and be inserted into the trap. Though the source was designed without cooling, multiple shots do not impart a great deal of thermal energy to the mass of the ion

source. Therefore, if a single shot proves incapable of providing the number of ions needed for the experiment, successive shots can be taken until the needed density is achieved.

The actual charge state of the ions coming from the source was left undetermined, though we anticipate the majority of the ions coming from the source to be singly ionized, given the amount of energy available and the large number of ions being released. Once assembled into the trap itself, testing can be performed to see just what states are present and in what quantities, and further adjustments can be made at that time to select particular charge states.

The velocity of the ions from the source matches typical velocities measured in other MeVVA source designs. Our testing shows it appears to be independent of the voltage bias applied to the cathode, and is rather a function of the arc discharge and the ions themselves. The velocities attained are within the range of confineable energies.

5.3 Surface Behavior

Examination of the surface revealed that ablation occurs across the entire unmasked region of the source, and to good depths. The source should have no difficulty removing ^{7}Be from the surface of the boron carbide target. Though in reality only small quantities of material are removed at a time, it is unclear what effect prolonged use has on the target. Eventually the surface will be extremely uneven, and the effect of that type of surface on the performance of the ion source is unknown. We may likely never really know what happens in that case, because we have a large number of boron carbide targets available for use in the experiment.

The behavior of the remaining surface is quite interesting, and it remains to be

exactly determined just what is occurring. The restructuring and crystallizing of the surface certainly appears to have no effect on the performance of the ion source, however, and is more a curiosity than an issue for this particular experiment.

5.4 Conclusions

The need to experiment with a plasma undergoing radioactive decay presents some challenging problems in design and implementation. The ion source we have developed addresses a good number of those concerns successfully. It is suitable for use in an ultra high vacuum environment while remaining easily removable and interchangeable. This setup allows us to change target samples for continued experiments without having to repressurize the entire trap system.

As an added benefit, the design allows for a great deal of flexibility in ion species. By simply making a disk of any conductive material the same size and shape as the boron carbide targets we use now, we could use the same ion source for other types of metals, radioactive or not. This feature will give our research group the added benefit of having a pre–built trap and ion source for a number of different types of plasma experiments.

Our testing of the source shows it to be an effective means of extracting ^{7}Be ions from the surface of a boron carbide target, and provides a stream of ions at confineable energies. Once placed inside our trap system, the ion source will help us to create a ^{7}Be plasma that can be studied for time scales on the order of its half-life. Examining this plasma will help us understand radioactive decay of this isotope better, while providing insight into the presence of this isotope in our upper atmosphere.

Bibliography

[1] J. R. Arnold and H. Al-Salih, *H. Science*, **121**, 451 (1955).

[2] L. Husain, P. E. Coffey, R. E. Meyers, and R. T. Cederwall, *Geophys. Res. Lett.*, **4**,363 (1977).

[3] N. Bhandari, *J. Geophys. Res.*, **75**, 2927 (1970).

[4] M. H. Shapiro and J. L. Forbes–Resha, *J. Geophys. Res.*, **81**, 2647 (1976).

[5] D. E. Walling, Q. He, and W. Blake, *Water Resources Research*, **35**, 3865 (1999).

[6] S. A. Fitgerald et al., *Environ. Sci. Technol.*, **35**, 300 (2001).

[7] C. Dueñas et al., *Atmospheric Environment*, **33**, 3705 (1999).

[8] P. A. Voytas et al., *Phys. Rev. Lett.*, **88**(1), 012501 (2002).

[9] A. Ray et al., *Phys. Rev. C*, **66**, 012501 (2002).

[10] H. W. Johlige, D. C. Aumann, and H. J. Born, *Phys. Rev. C*, **2**, 1616 (1970).

[11] C. A. Huh, *Earth Planet Sci. Lett.*, **171**, 325 (1999).

[12] G. J. Fishman et al., *Nature*, **349**, 678 (1991).

[13] G. H. Share and R. J. Murphy, *Astrophys. J.*, **485**, 409 (1997).

[14] G. W. Petty, *Geophys. Res. Lett.*, **18**, 1687 (1991).

[15] G. W. Phillips et al., *Geophys. Res. Lett.*, **28**, 939 (2001).

[16] J. H. Malmberg and J. S. deGrassie, *Phys. Rev. Lett.*, **35**, 577 (1975).

[17] R. W. Gould, *Phys. Plasmas*, **2**, 2151 (1995).

[18] B. Asamoto, FT–ICR/MS: analytical applications of fourier transform ion cyclotron resonance mass spectrometry, VCH Publishers, New York, 1991.

[19] D. K. Olson, Undergraduate Senior Thesis, Brigham Young University Department of Physics and Astronomy ,2005.

[20] R. J. Peterson et al., Ann. of Nucl. Energy, **2**, 503 (1975).

[21] I. G. Brown, J. E. Galvin, and R. A. MacGill, Appl. Phys. Lett., **47**, 358 (1985).

[22] I. G. Brown, The Physics and Technology of Ion Sources, (Wiley, New York, 1989)

[23] C. D. Child, Phys. Rev. (Ser. 1), **32**, 492 (1911).

[24] I. Langmuir and K. T. Compton, Rev. Mod. Phys., **3**, 191 (1931).

[25] I. G. Brown, J. E. Galvin and R. A. MacGill, Rev. Sci. Instrum., **57**, 1069 (1986).

[26] I. G. Brown, J. E. Galvin, R. A. MacGill and R. T. Wright, Appl. Phys. Lett., **49**, 1019 (1986).

[27] I. G. Brown, J. E. Galvin and R. A. MacGill, Rev. Sci. Instrum., **61**, 577 (1990).

[28] R. A. MacGill, I. G. Brown and J. E. Galvin, Rev. Sci. Instrum., **61**, 580 (1990).

[29] H. Shiraishi and I. G. Brown, Rev. Sci. Instrum., **61**, 589 (1990).

[30] H. Shiraishi and I. G. Brown, Rev. Sci. Instrum., **61**, 3775 (1990).

[31] G. E. Holland et al., Rev. Sci. Instrum., **76**,073304 (2005).

[32] I. G. Brown, (private correspondence).

Appendix A

Machining Drawings

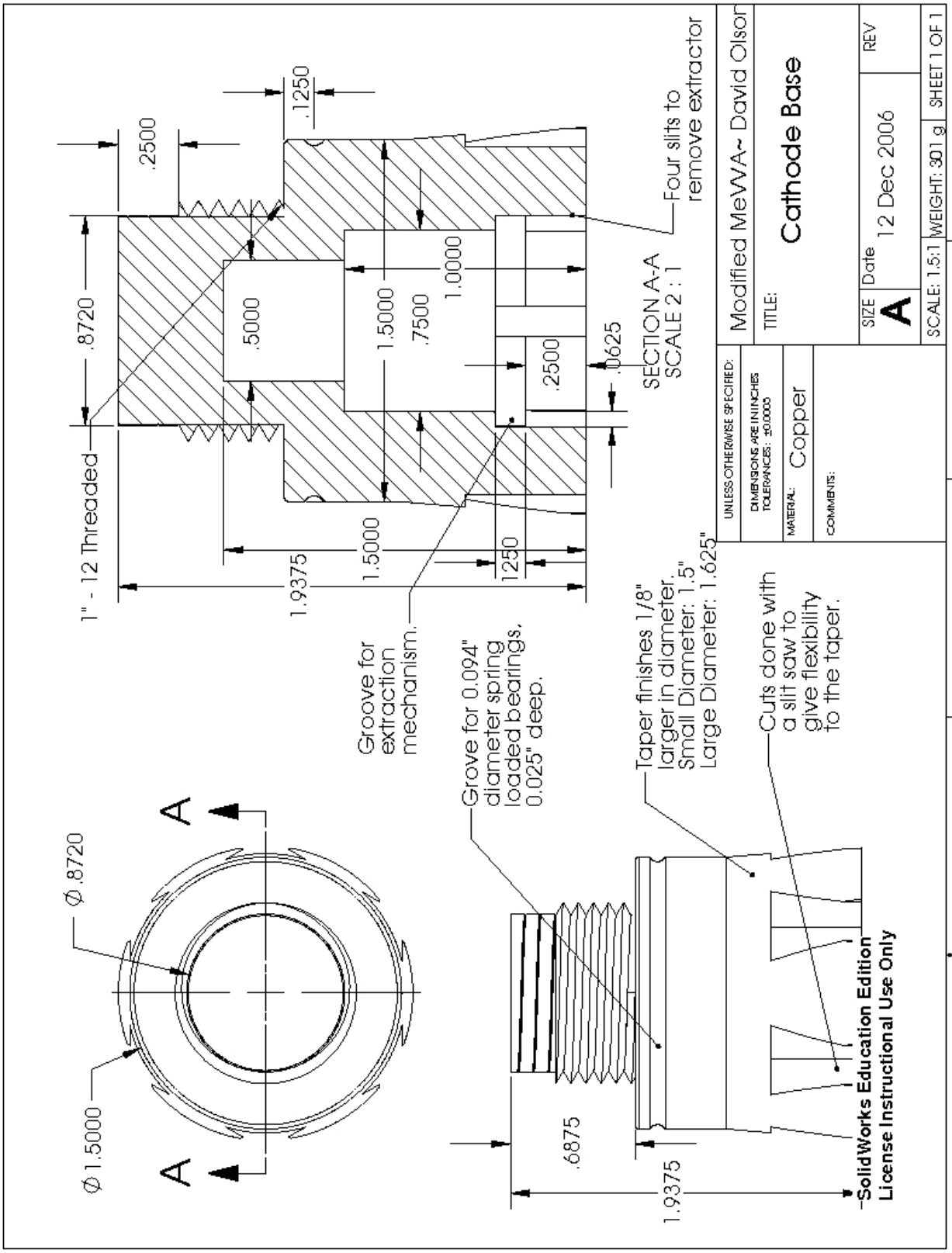

Figure A.1 Cathode Base Machining Drawing

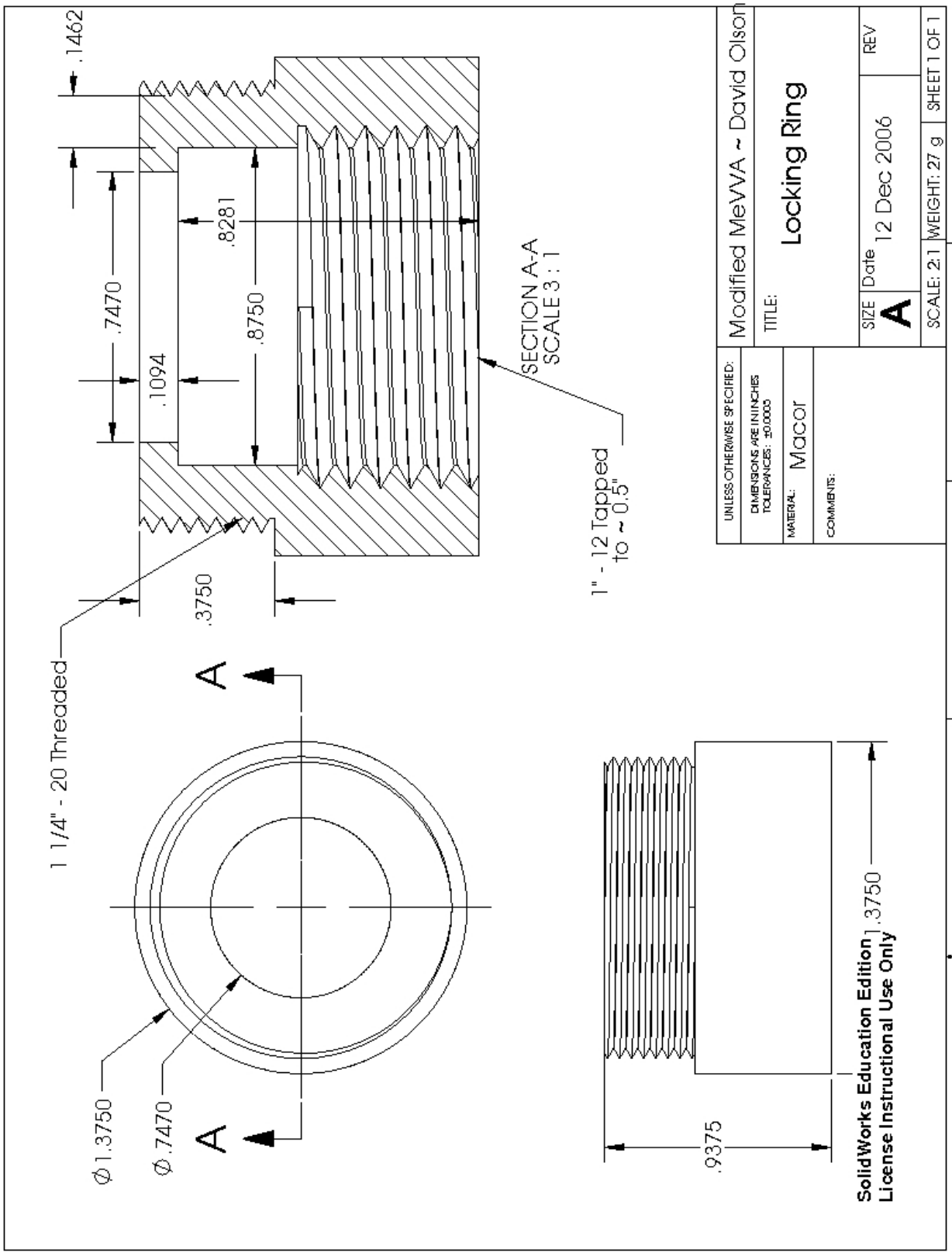

Figure A.2 Locking Ring Machining Drawing

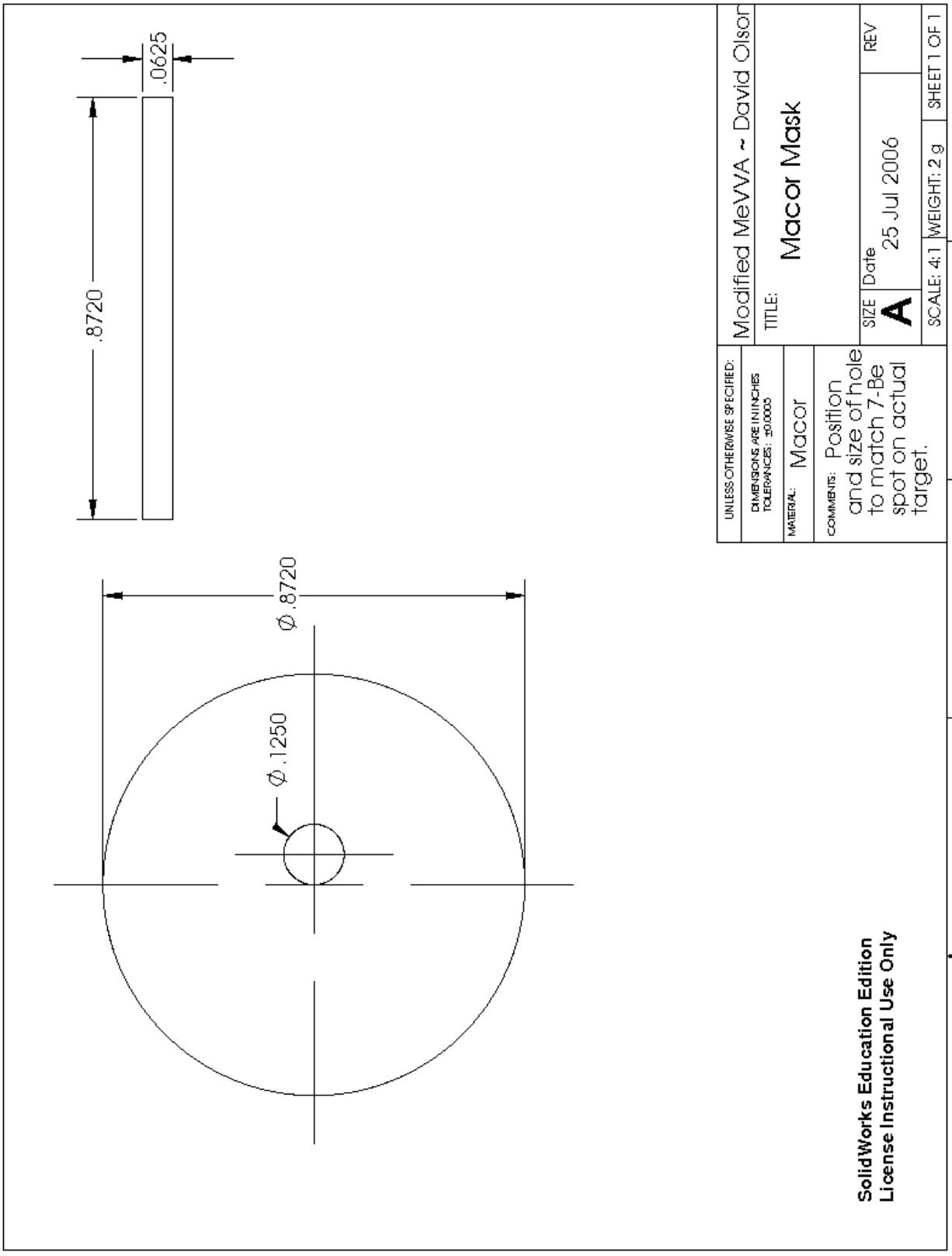

Figure A.3 Macor Mask Machining Drawing

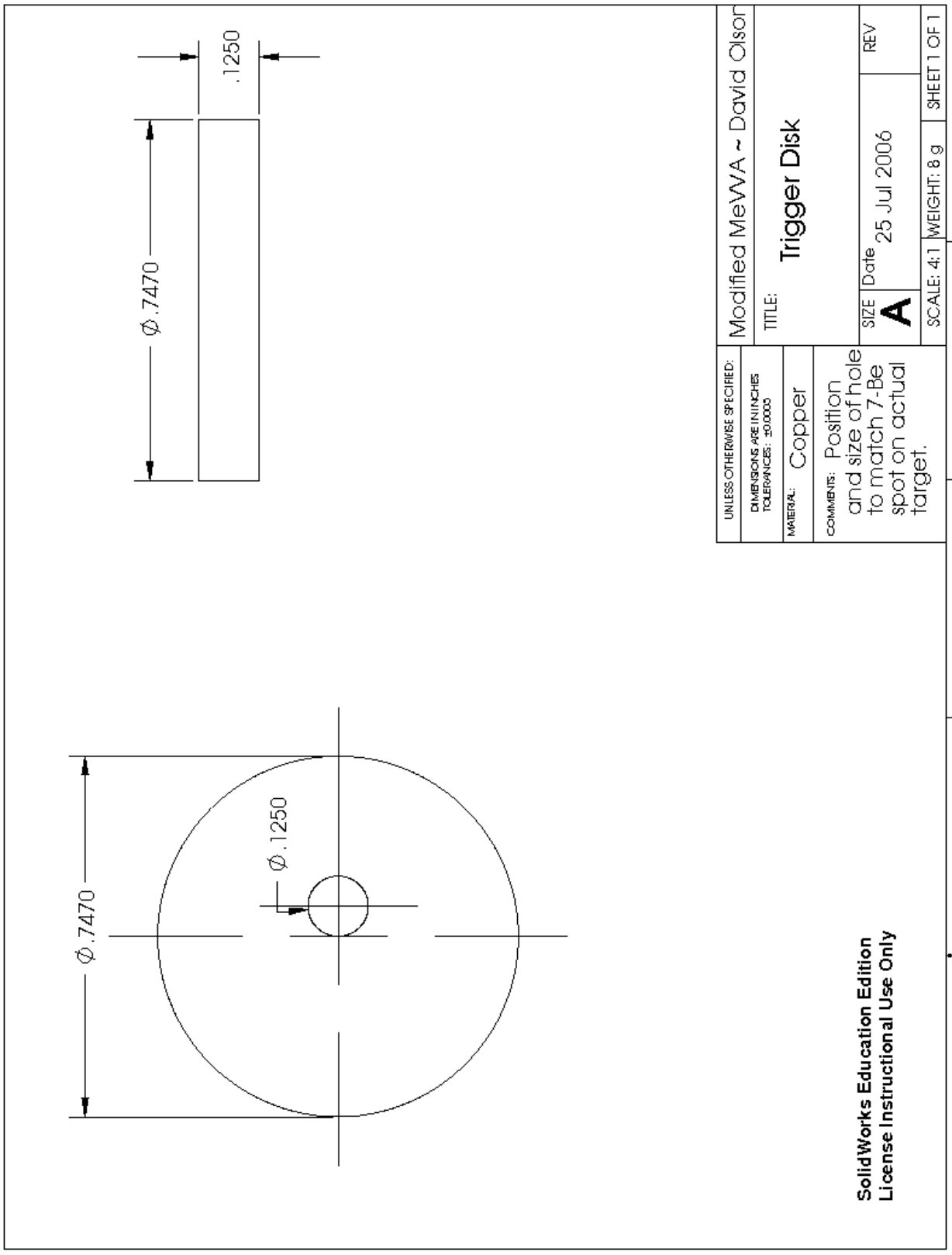

Figure A.4 Trigger Disk Machining Drawing

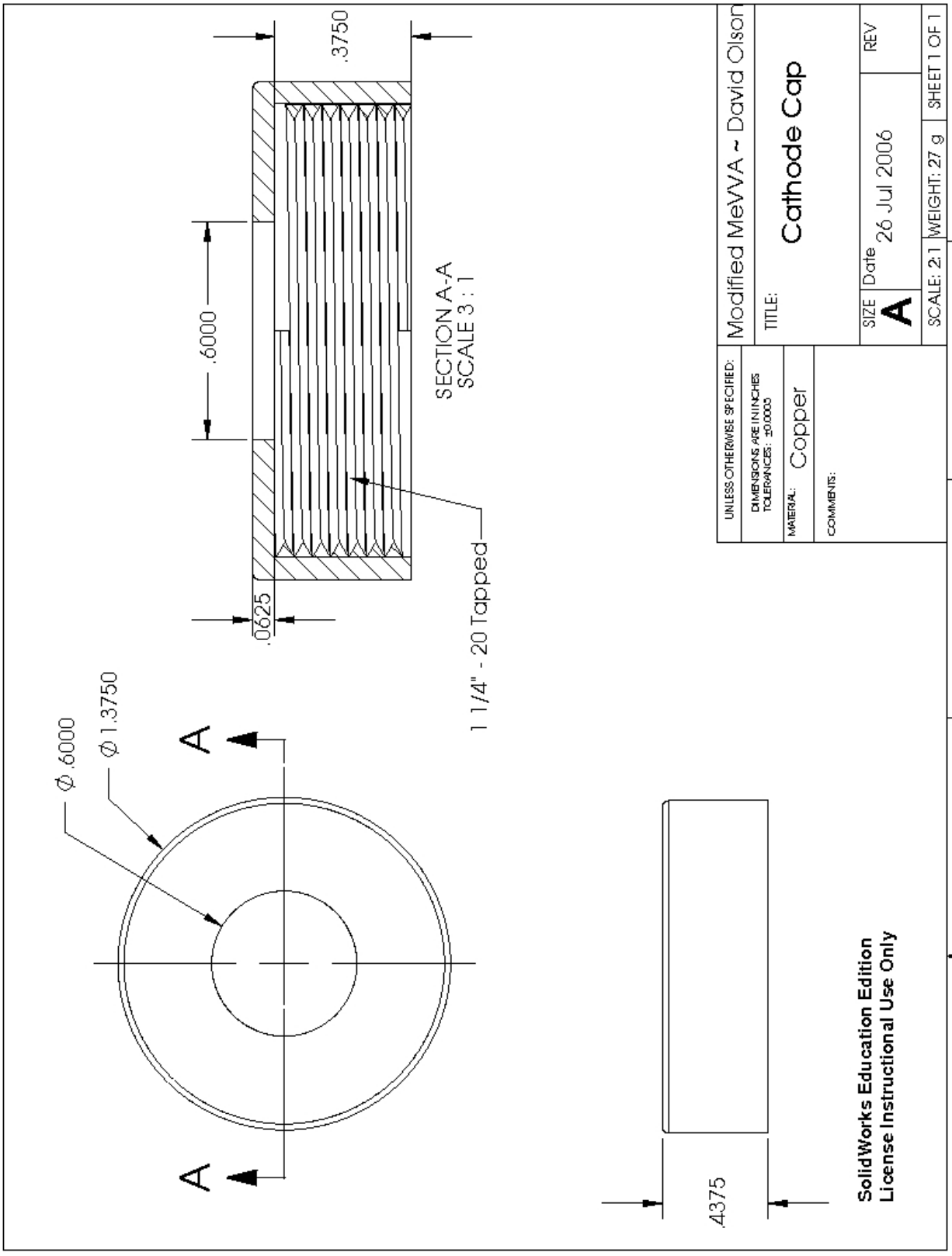

Figure A.5 Cathode Cap Machining Drawing

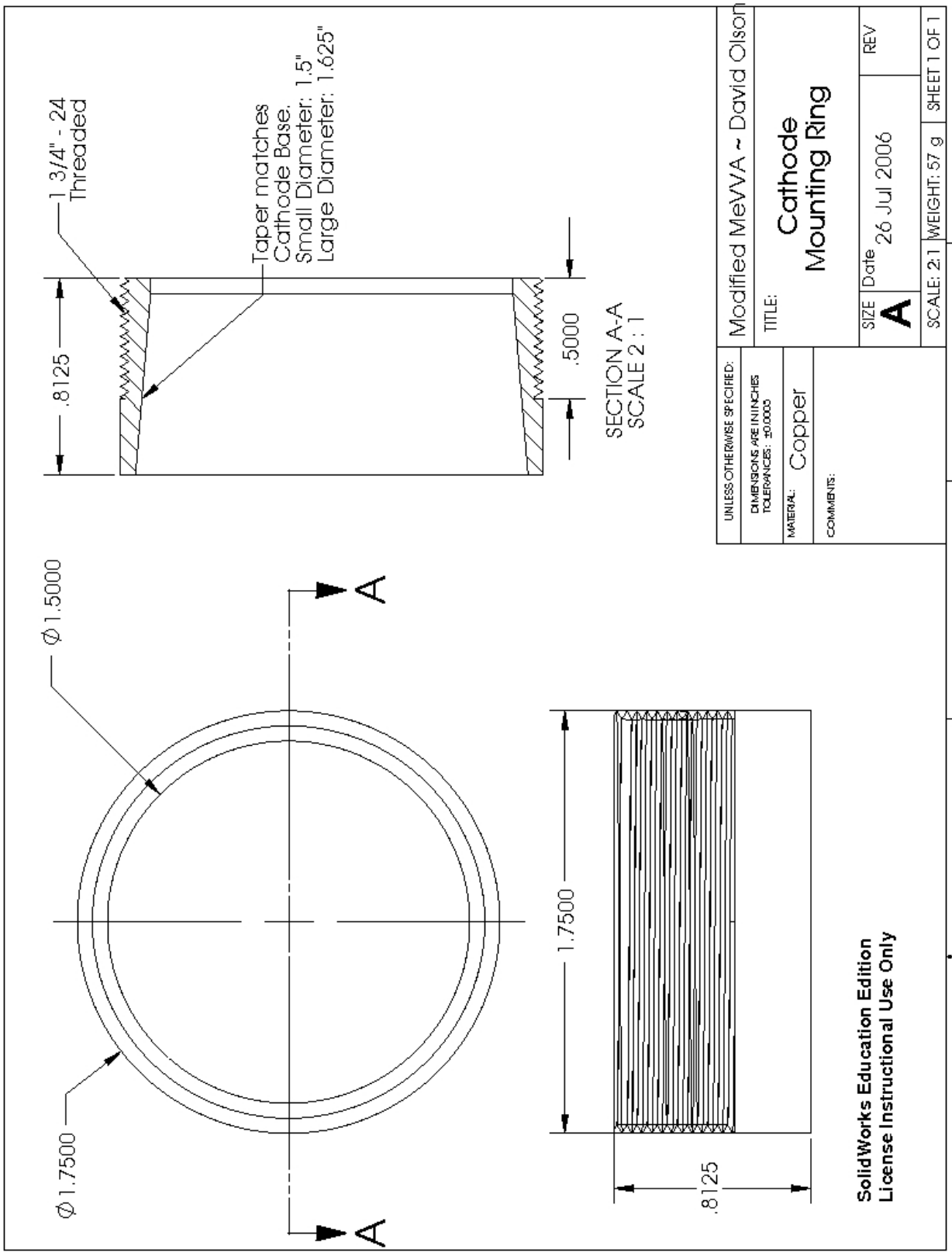

Figure A.6 Cathode Mounting Ring Machining Drawing

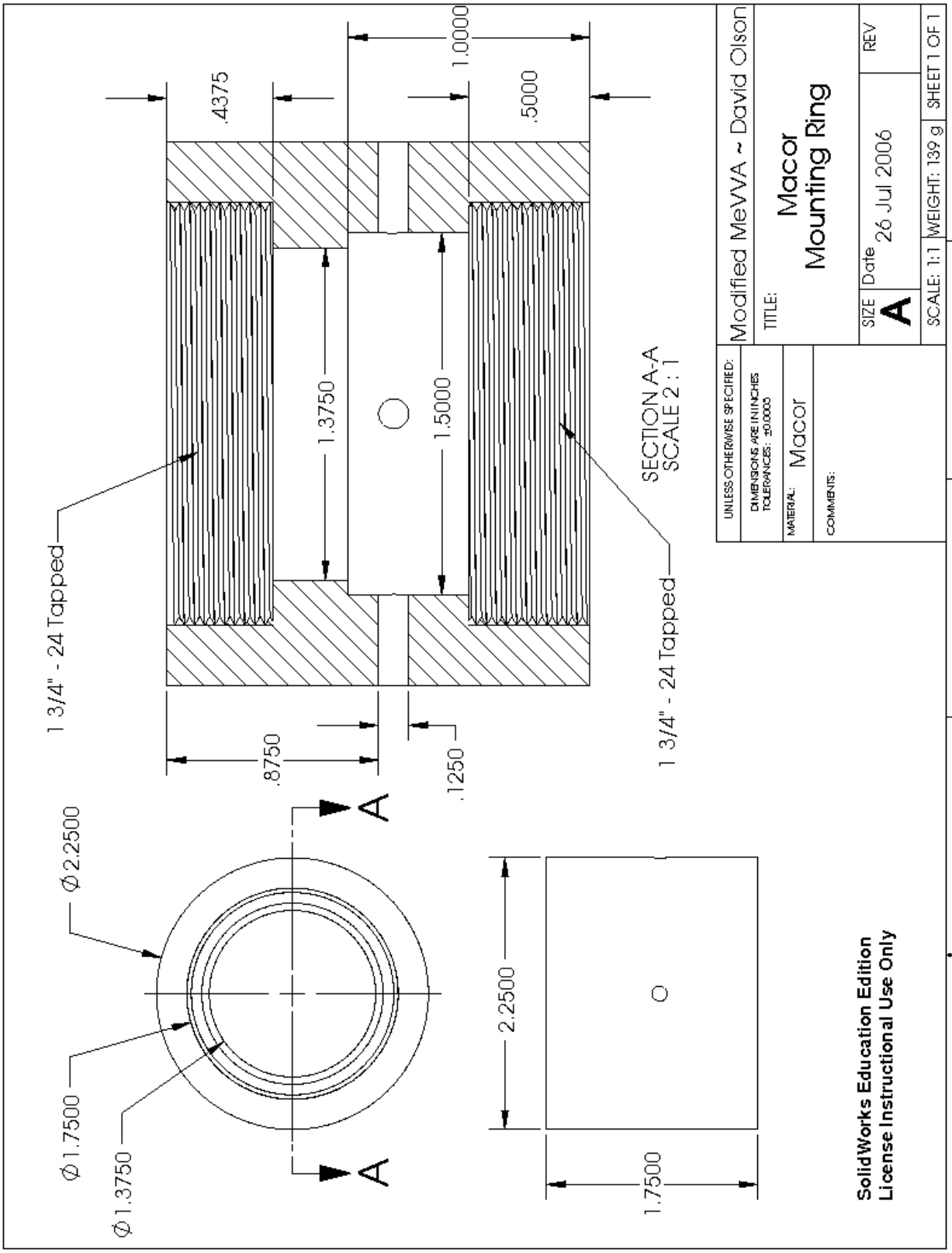

Figure A.7 Macor Mounting Ring Machining Drawing

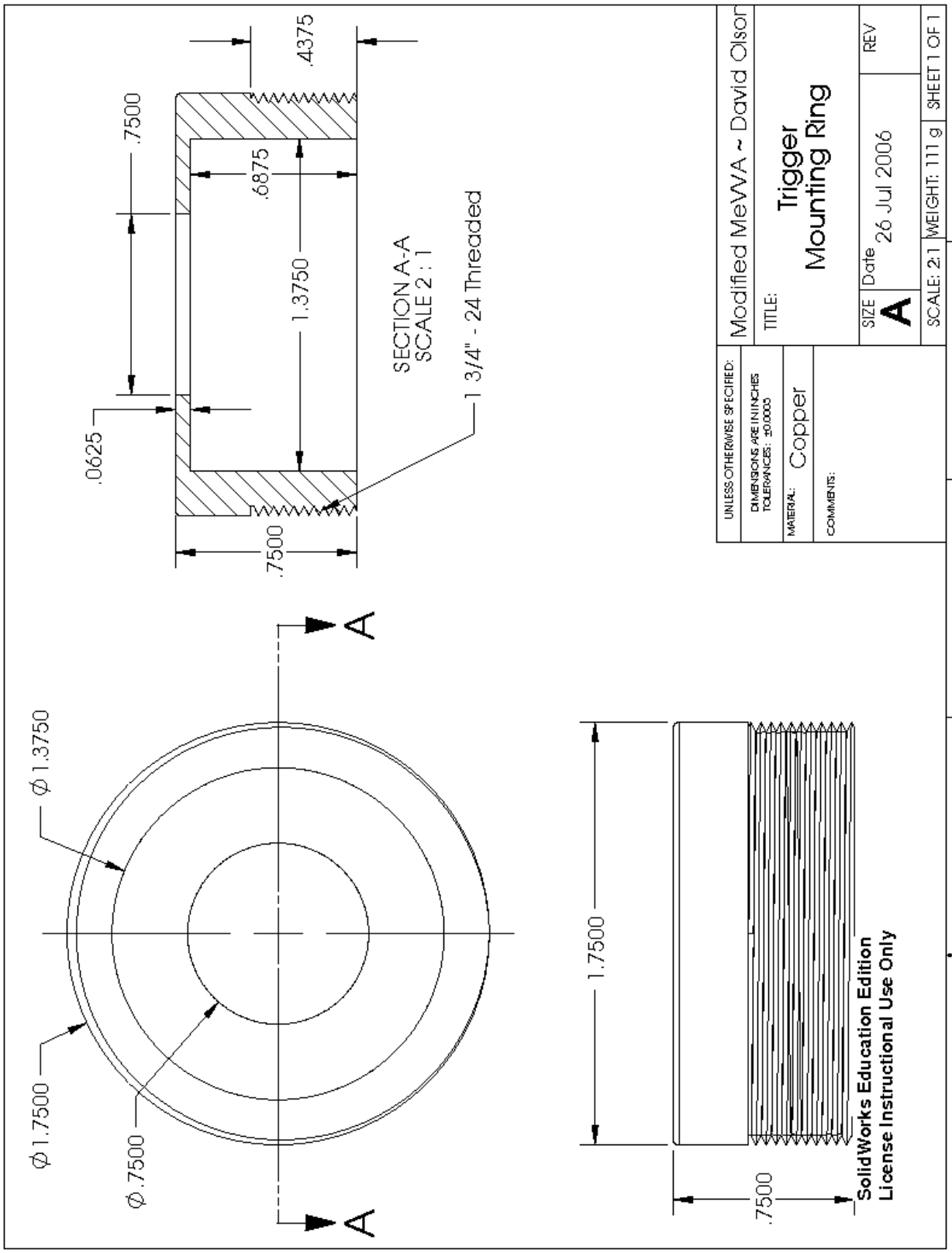

Figure A.8 Trigger Mounting Ring Machining Drawing

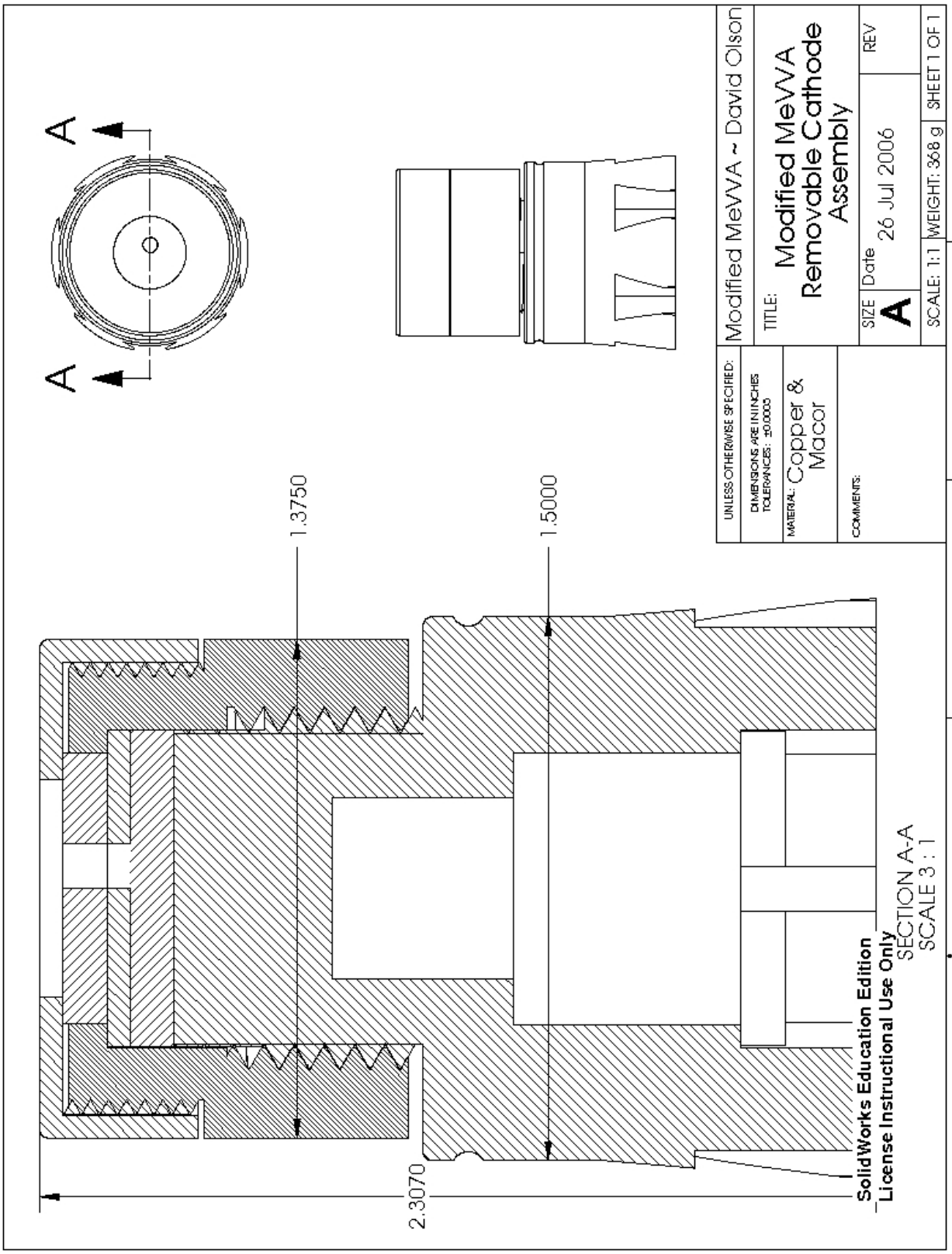

Figure A.9 Cathode Assembly Diagram

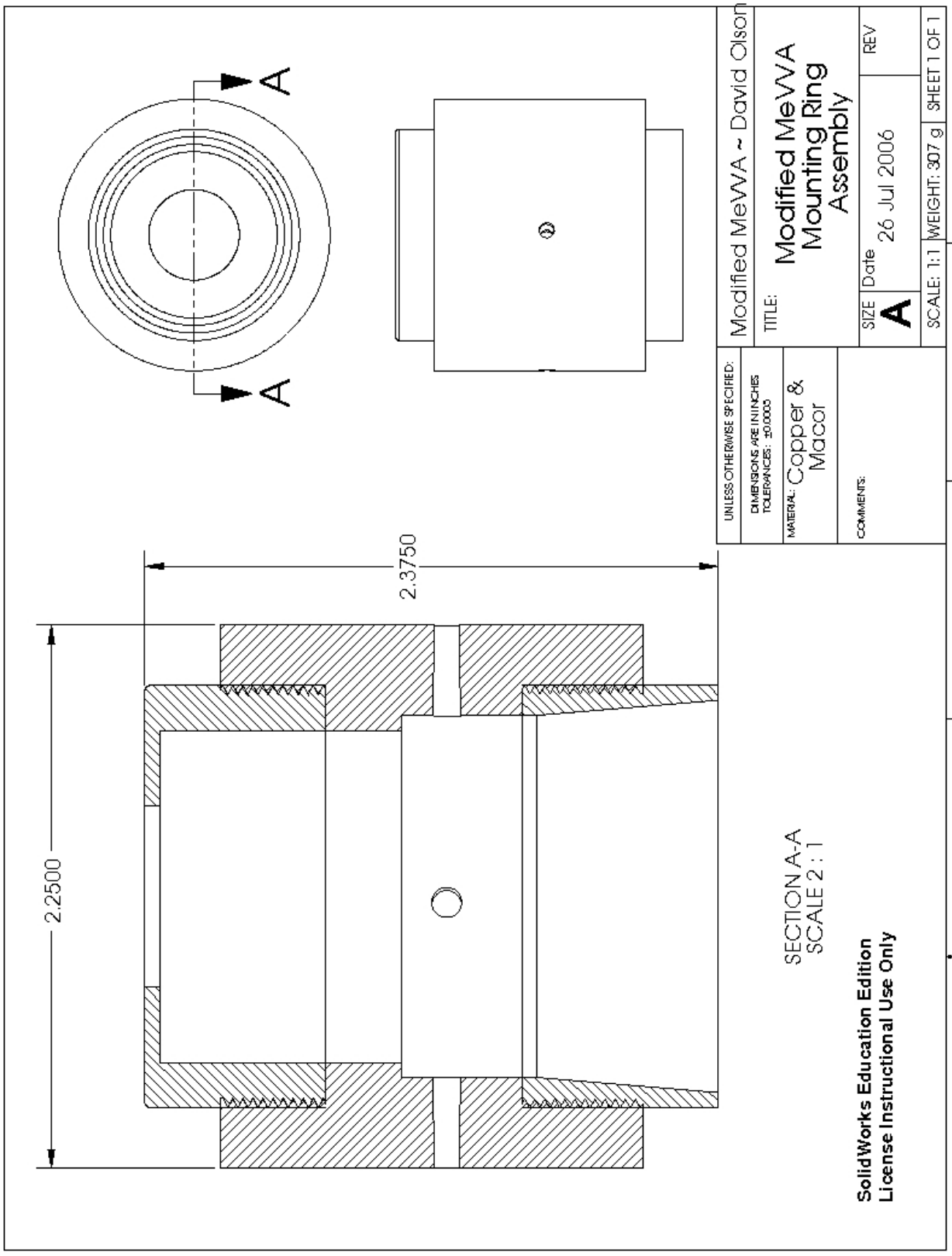

Figure A.10 Mounting Rings Assembly Diagram

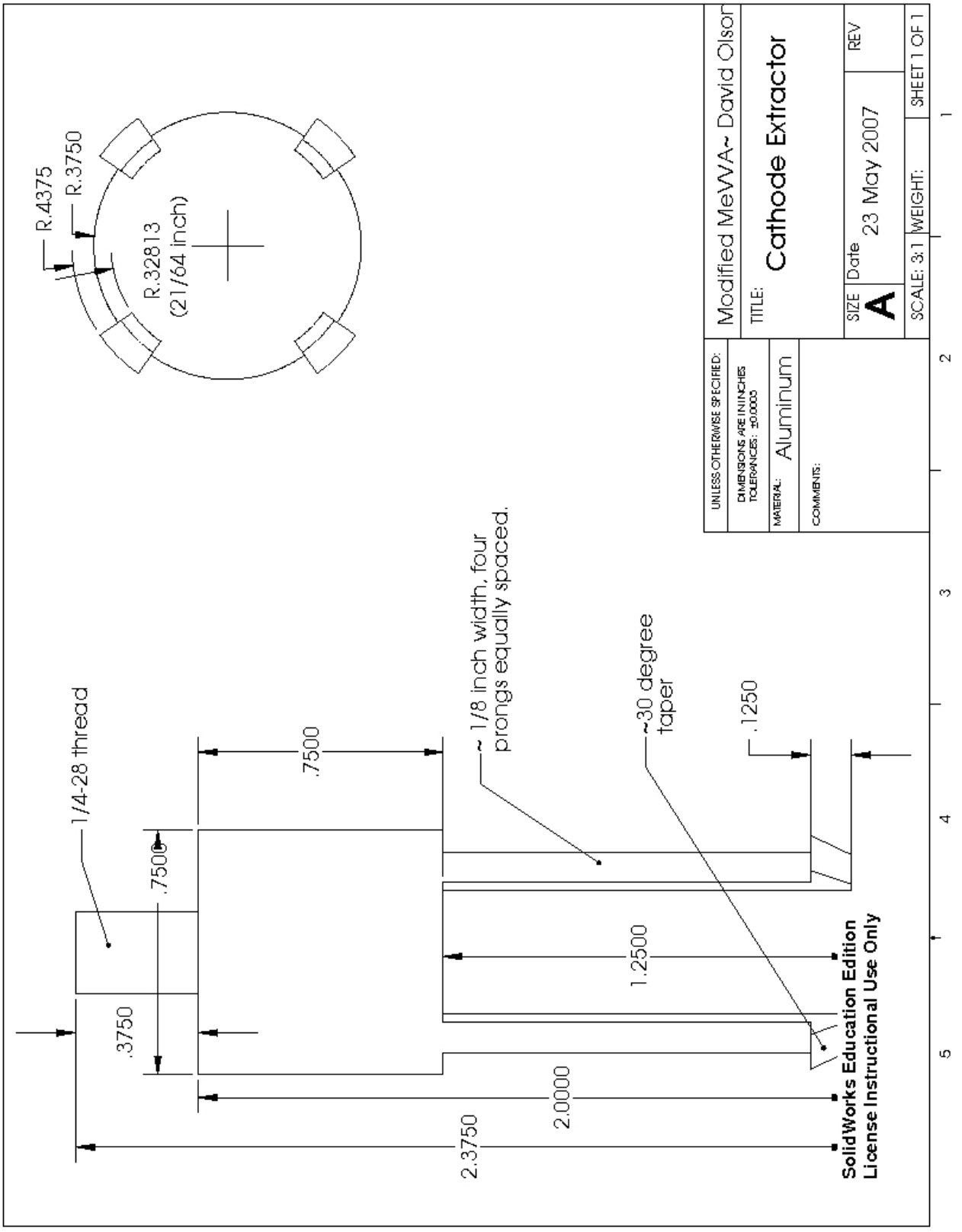

Figure A.11 Extractor Machining Drawing

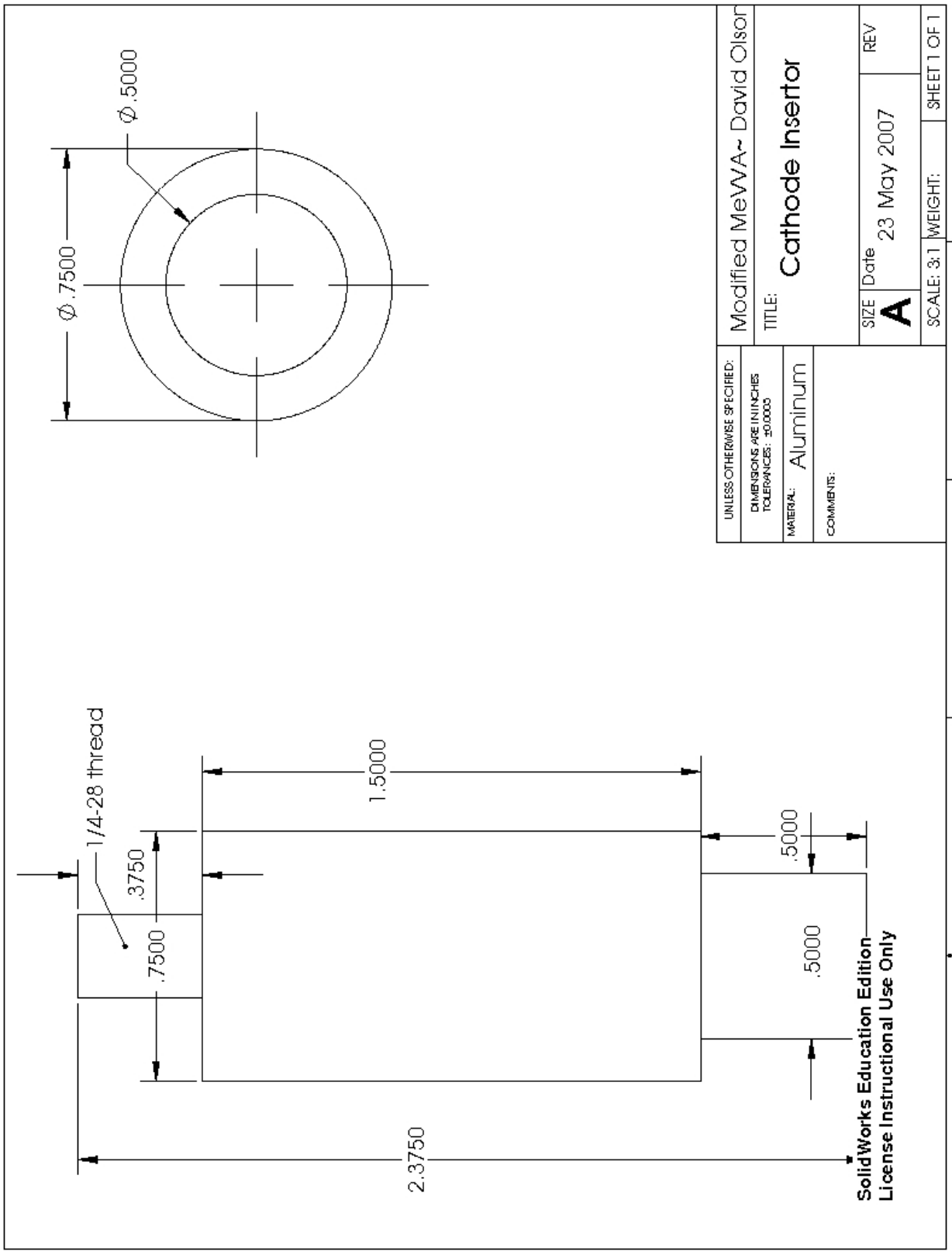

Figure A.12 Insertor Machining Drawing

Appendix B

Circuit Diagrams

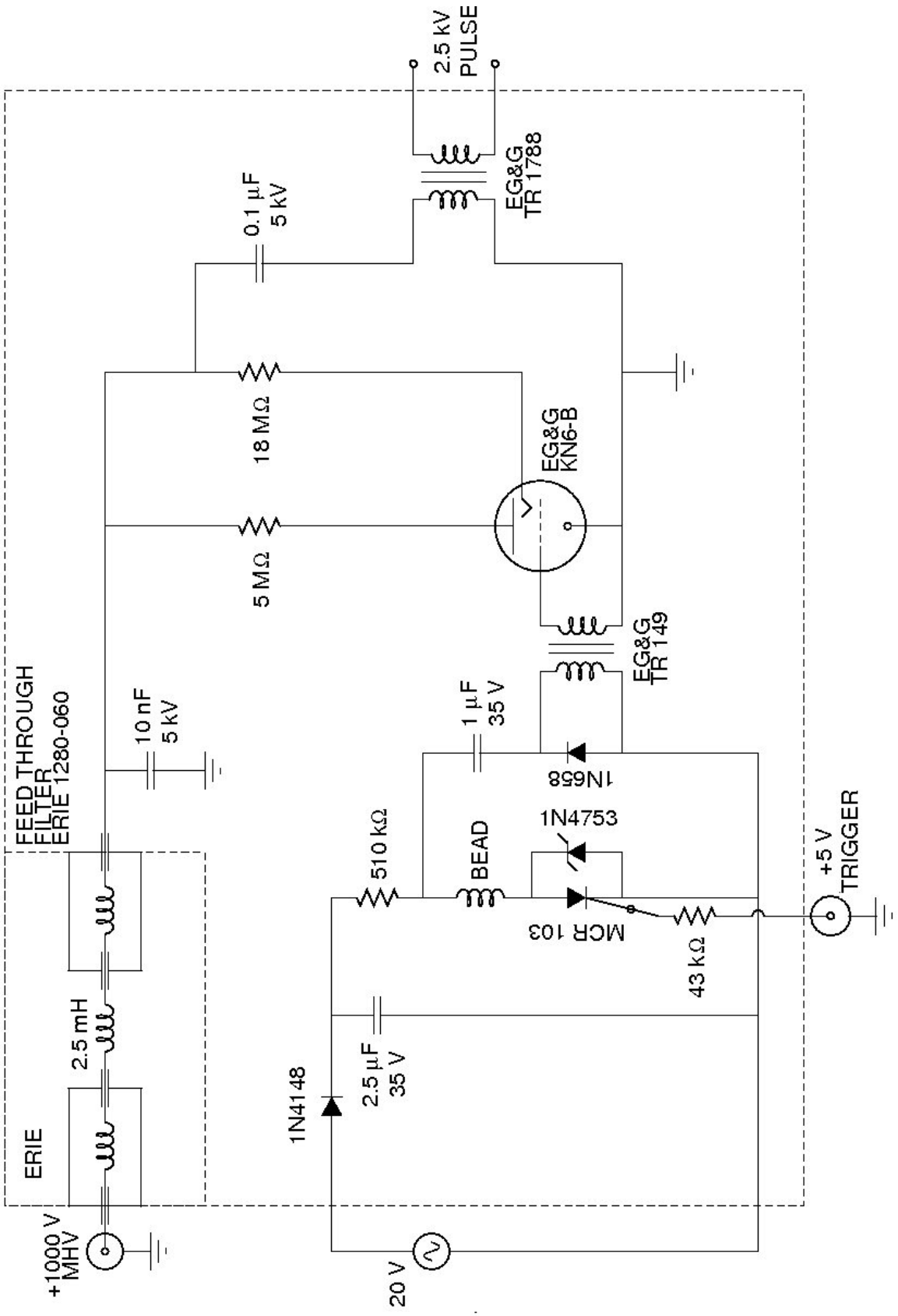

Figure B.1 The HV Trigger Pulse Generator

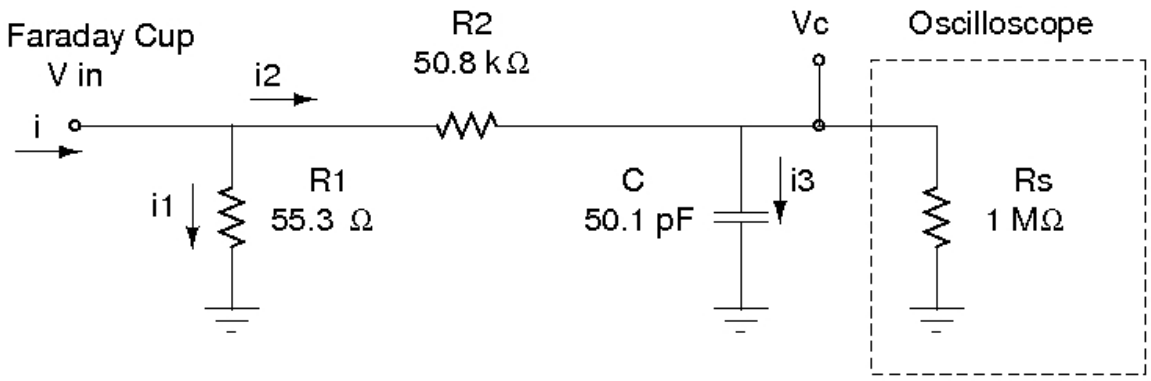

Figure B.2 The Passive Integrator Circuit

Appendix C

Computer Analysis Code

```
%  plotter.m
%
%  This program loads data recorded by the oscilloscopes, adjusts the
%  timing to plot different shots together, and smooths the data to
%  make nice, printable graphs for publication.
%
%  Copyright 2007, David K. Olson
%
%%%%%%%%%%%%%%%%%%%%%%%%%%%%%%%%%%%%%%%%%%%%%%%%%%%%%%%%%%%%%%%%

clear;  close all;

%  Define the directory where data is found and the files being used

dataset='/home/david/research/ion source/Data/Data 2007March26/';
file1=[dataset 'fire022'];
file2=[dataset 'fire022'];
file3=[dataset 'fire007'];
% file4=[dataset 'fire016'];
% file5=[dataset 'fire021'];

data1=load([file1 'HV.dat']);
data2=load([file2 'channel2.dat']);
data3=load([file3 'channel2.dat']);
% data4=load([file4 'channel2.dat']);
% data5=load([file5 'channel2.dat']);

% data40=load([file40 'channel4.dat']);
% trig40=load([file40 'trigger.dat']);


%  Scale data for comparison, if necessary.

scale1=data1(:,2)/max(data1(:,2));
scale2=data2(:,2)/max(data2(:,2));
scale3=data3(:,2)/max(data3(:,2));
% scale4=data4(:,2);%/max(data4(:,2));
% scale5=data5(:,2);%/max(data5(:,2));


%  Because the electronics have random delays before discharging, the
%  data is aligned according to the initial noise pulse from the spark
%  gap discharge.  The rising edge is found, and the times at which
```

```
%  they occur for each file are compared to find delays.

i1=min(find(scale1>0.1 & scale1<0.2));
i2=min(find(scale2>0.1 & scale2<0.2));
i3=min(find(scale3>0.1 & scale3<0.2));
% i4=min(find(scale4>0.5 & scale4<0.7));
% i5=min(find(scale5>0.5 & scale5<0.7));

dmin=min([data1(i1,1) data2(i2,1) data3(i3,1)]);% data4(i4,1) data5(i5,1)]);

d1=data1(i1,1)-dmin;
d2=data2(i2,1)-dmin;
d3=data3(i3,1)-dmin;
% d4=data4(i4,1)-dmin;
% d5=data5(i5,1)-dmin;


%  Plotting the data together

figure
plot(data1(:,1)-d1,scale1,'r-')
hold on
plot(data2(:,1)-d2,scale2,'b-')
plot(data3(:,1)-d3,scale3,'k-')
% plot(data4(:,1)-d4,scale4,'g-')
% plot(data5(:,1)-d5,scale5,'m-')
hold off


%  Smoothing algorithm, takes the average of groups of n1 to reduce
%  noisy oscillations.  There is also the ability to scale data from
%  two separate oscilloscopes, since the computer records different
%  length arrays from the individual scopes.

N1=length(scale1);
% N2=length(scale2);
n1=50;
% n2=5;
j=1;

ts1=zeros(floor(N1/n1),1);
ts2=ts1; ts3=ts1; ts4=ts1; ts5=ts1;
s1=ts1; s2=ts1; s3=ts1; s4=ts1; s5=ts1;
```

```
while j<=floor(N1/n1)
    ts1(j)=mean(data1((j-1)*n1+1:j*n1,1));
    ts2(j)=mean(data2((j-1)*n1+1:j*n1,1));
    ts3(j)=mean(data3((j-1)*n1+1:j*n1,1));
%     ts4(j)=mean(data4((j-1)*n1+1:j*n1,1));
%     ts5(j)=mean(data5((j-1)*n1+1:j*n1,1));
    s1(j)=mean(scale1((j-1)*n1+1:j*n1));
    s2(j)=mean(scale2((j-1)*n1+1:j*n1));
    s3(j)=mean(scale3((j-1)*n1+1:j*n1));
%     s4(j)=mean(scale4((j-1)*n1+1:j*n1));
%     s5(j)=mean(scale5((j-1)*n1+1:j*n1));

    j=j+1;
end

% j=1;
% while j<=floor(N2/n2)
% %     ts1(j)=mean(data1((j-1)*n2+1:j*n2,1));
%     ts2(j)=mean(data2((j-1)*n2+1:j*n2,1));
% %     ts4(j)=mean(data4((j-1)*n2+1:j*n2,1));
%
% %     s1(j)=mean(scale1((j-1)*n2+1:j*n2));
%     s2(j)=mean(scale2((j-1)*n2+1:j*n2));
% %     s4(j)=mean(scale4((j-1)*n2+1:j*n2));
%
%     j=j+1;
% end


%  Plot the smoothed data

figure
plot(ts1-d1,s1,'r-');
hold on
plot(ts2-d2,s2,'b-');
plot(ts3-d3,s3,'k-');
% plot(ts4-d4,s4,'g-');
% plot(ts5-d5,s5,'m-');
hold off


%  Extra code used to find velocities based on the data
```

```
ix1=min(find(s1>0.09 & s1<0.11));
ix2=min(find(s2>0.09 & s2<0.11));
ix3=min(find(s3>0.09 & s3<0.11));

v1=0.14/(ts1(ix1)-data1(i1,1))
v2=0.25/(ts2(ix2)-data2(i2,1))
v3=0.40/(ts3(ix3)-data3(i3,1))
```

```
%  pier2.m
%
%  This is the passive integration effect reversal code.  This takes
%  data obtained from a faraday cup signal through a passive integrator
%  and calculates what the charge input must have been to obtain the
%  observed signal.
%
%  Copyright 2007, David K. Olson
%
%%%%%%%%%%%%%%%%%%%%%%%%%%%%%%%%%%%%%%%%%%%%%%%%%%%%%%%%%%%%%%%%%%%%

clear; close all;

%  Define the directory where data is found

dataset='/home/david/research/ion source/Data/AFM Prep Data/';


%  The values of the components in the passive integrator

R1=55.3;  R2=50.8e3;  Rs=1e6;  C=50.1e-12;


%  Load data.  The option here loads a set of shots labeled fire001
%  through fire025.  Removing the for loop allows examining only one
%  single shot.

for a=1:25
    file=num2str(a, '%03.3d');
    data=load([dataset 'fire' file 'channel2.dat']);
    t=data(:,1);
    Vc=data(:,2);
    N=length(Vc);


%  Smoothing algorithm.  The first two commented lines were used in
%  analyzing the smoothing effects on the data by comparing values of
%  Q obtained by averaging groups of 50 to 500 at a time.

%     for k=1:46
%         n=50+(k-1)*10;

    n=10;
```

```
    Ns=floor(N/n);
    ts=zeros(Ns,1);
    Vcs=ts;   Vcp=ts;

    for j=1:Ns
        Vcs(j)=mean(Vc( (1+n*(j-1)):n*j ));
        ts(j)=mean(t( (1+n*(j-1)):n*j ));
    end


%  Centered difference method for calculating the derivative.  The end
%  points use forward and backward difference methods.

    Vcp(1)=(Vcs(2)-Vcs(1))/(ts(2)-ts(1));
    for j=2:Ns-1
        Vcp(j)=(Vcs(j+1)-Vcs(j-1))/(ts(j+1)-ts(j-1));
    end
    Vcp(Ns)=(Vcs(Ns)-Vcs(Ns-1))/(ts(Ns)-ts(Ns-1));


%  Calculation of current in
    I=(R1+R2+Rs)/R1/Rs*Vcs+(R1+R2)*C/R1*Vcp;

%  Calculation of charge in by integration
    Q(a)=trapz(ts,I);

%  Print results
    fprintf(['fire ' file ': Q = %g \t N = %g \n'], Q(a), Q(a)/1.6022e-19);
end

    % plot(50:10:500,Q)


%  Calculate average and standard deviation for analyzing multiple
%  shots.

fprintf('-------------------------\n');
fprintf('mean Q = %g \t std Q = %g \n',mean(Q),std(Q));
fprintf('mean N = %g \t std Q = %g \n',mean(Q)/1.6022e-19,std(Q)/1.6022e-19);

plot(Q)
figure
plot(Q/1.6022e-19)
```

Appendix D

Data Analysis

D.1 Reverse Integrator

Using Kirchoff's loop rules on the integrator circuit (Page refpagefig:intc), we find the following set of equations:

$$i = i_1 + i_2 \tag{D.1}$$

$$V_c = R_1 i_1 - R_2 i_2 \tag{D.2}$$

$$\frac{V_c}{R_s} = i_2 - i_3 \tag{D.3}$$

$$i_3 = CV_c' \tag{D.4}$$

These equations form a set of Differential-Algebraic Equations that govern the system. The oscilloscope measures V_c, and so it can be used as an input in solving for the intitial current i. The following Maple code shows that the solution to the set of equations is:

$$i = \frac{R_1 + R_2 + R_s}{R_1 R_s}\, V_c \;+\; \frac{R_1 + R_2}{R_1}\, C\, V_c' \tag{D.5}$$

The equation requires knowing the time derivative of V_c, and so smoothing of the data (discussed in section D.2) is required to get good numerical derivatives when computing the input current.

Knowing the input current as a function of time allows us to calculate the total charge input by simple integration.

pler.mw

This maple code solves the DAE system for the passive integrator circuit symbolically.
The equation needed is located as the first element of the final equation.


```
restart; with(LinearAlgebra) :
A := Matrix([[1,-1,-1, 0], [0,R1,-R2, 0], [0, 0, 1,-1], [0, 0, 0, 1]]);
```

$$\begin{bmatrix} 1 & -1 & -1 & 0 \\ 0 & R1 & -R2 & 0 \\ 0 & 0 & 1 & -1 \\ 0 & 0 & 0 & 1 \end{bmatrix} \tag{1}$$

```
f := Matrix([[0], [Vc], [Vc/Rs], [C·Vcp]]);
```

$$\begin{bmatrix} 0 \\ Vc \\ \frac{Vc}{Rs} \\ C\,Vcp \end{bmatrix} \tag{2}$$

```
x := Matrix([[i], [i1], [i2], [i3]]);
```

$$\begin{bmatrix} i \\ i1 \\ i2 \\ i3 \end{bmatrix} \tag{3}$$

```
Multiply(A, x) = f;
```

$$\begin{bmatrix} i - i1 - i2 \\ R1\,i1 - R2\,i2 \\ i2 - i3 \\ i3 \end{bmatrix} = \begin{bmatrix} 0 \\ Vc \\ \frac{Vc}{Rs} \\ C\,Vcp \end{bmatrix} \tag{4}$$

$Ap := MatrixInverse(A);$

$$\begin{bmatrix} 1 & \frac{1}{R1} & \frac{R1+R2}{R1} & \frac{R1+R2}{R1} \\ 0 & \frac{1}{R1} & \frac{R2}{R1} & \frac{R2}{R1} \\ 0 & 0 & 1 & 1 \\ 0 & 0 & 0 & 1 \end{bmatrix} \tag{5}$$

$x = Multiply(Ap, f);$

$$\begin{bmatrix} i \\ i1 \\ i2 \\ i3 \end{bmatrix} = \begin{bmatrix} \frac{Vc}{R1} + \frac{(R1+R2)\ Vc}{R1\ Rs} + \frac{(R1+R2)\ C\ Vcp}{R1} \\ \frac{Vc}{R1} + \frac{R2\ Vc}{R1\ Rs} + \frac{R2\ C\ Vcp}{R1} \\ \frac{Vc}{Rs} + C\ Vcp \\ C\ Vcp \end{bmatrix} \tag{6}$$

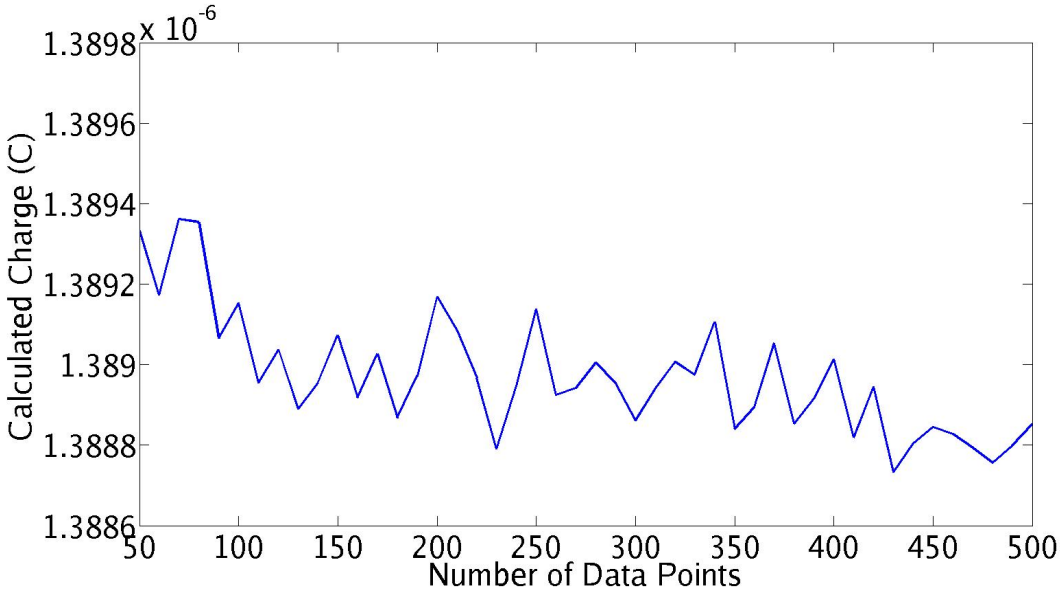

Figure D.1 Smoothing analysis for a typical shot with the cup at 25 cm. The x axis shows the number of data points included in an averaged group.

D.2 Data Smoothing

Data smoothing was employed both in calculating the amount of charge collected by the Faraday cup and in preparing plots for publication. Because of the quick signals, it was important to examine what effect data smoothing had on the calculation. A large number of data samples were examined by comparing the values of Q and N calculated in pier2.m using data point groups of 50 through 500 by 10. Figure D.1 shows a typical result. Larger groups do decrease the value calculated, as expected, but the change is only on the order of 0.01%.

Comparisons of all three cup distances used in measurements show little difference in the numerical behavior, as shown in table D.2.

Distance	mean Q	std. Q	mean N	std. N
14 cm	4.48844×10^{-06} C	5.58862×10^{-10} C	2.80142×10^{13}	3.48809×10^{09}
25 cm	1.38897×10^{-06} C	1.50307×10^{-10} C	8.66915×10^{12}	9.38132×10^{08}
40 cm	5.49762×10^{-07} C	9.28206×10^{-11} C	3.43129×10^{12}	5.79332×10^{08}

Table D.1 Means and Standard Deviations calculated to analyze smoothing effects on the Faraday cup data.

Appendix E

Project Photographs

E.1 Cathode Assembly

This section provides assembly instructions for all of the cathode parts.

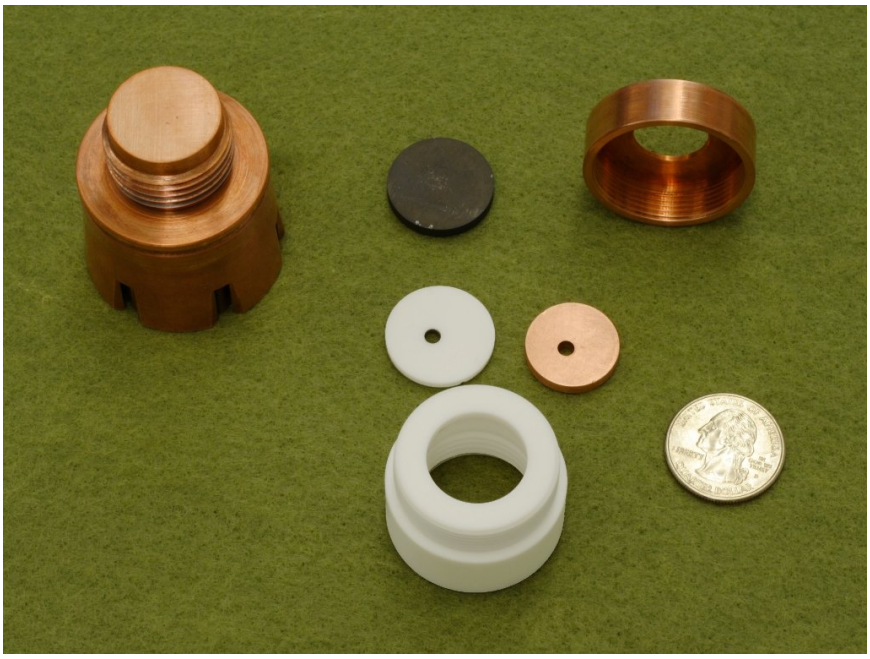

Figure E.1 All the individual pieces for the cathode.

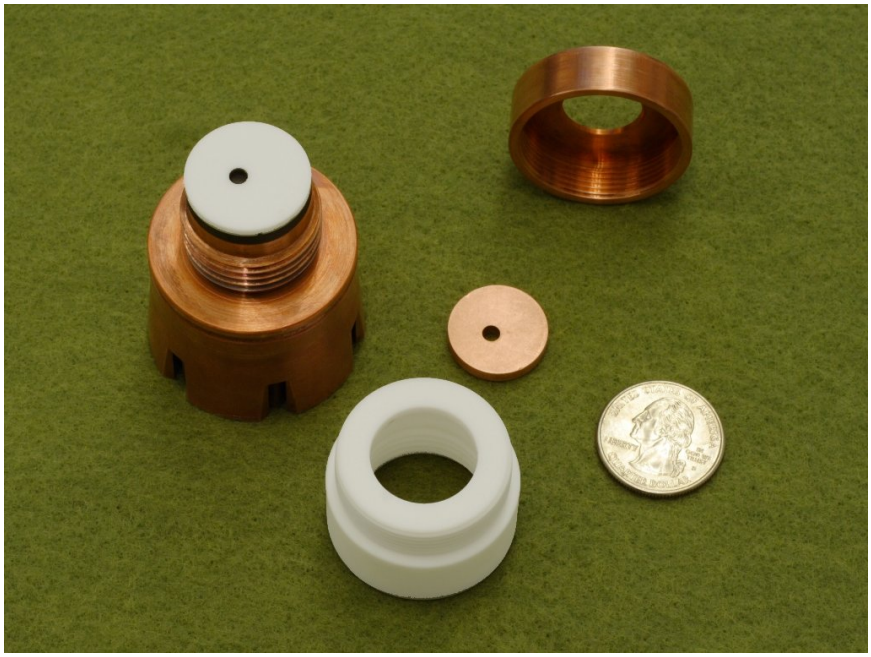

Figure E.2 The target and macor mask are placed onto the cathode base.

Figure E.3 The macor locking ring is tightened onto the mask.

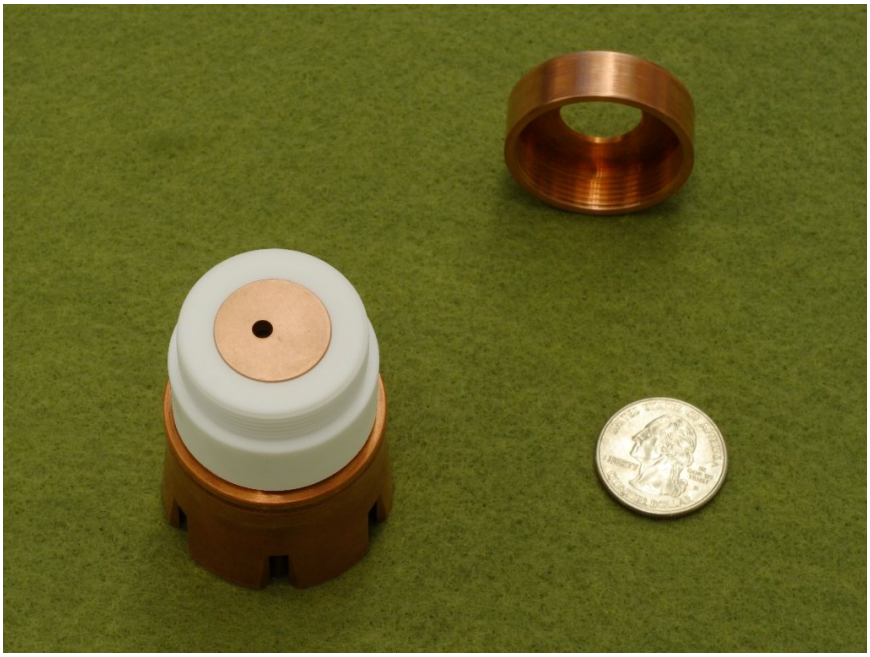

Figure E.4 The trigger disk is placed into the locking ring, aligned with the macor mask.

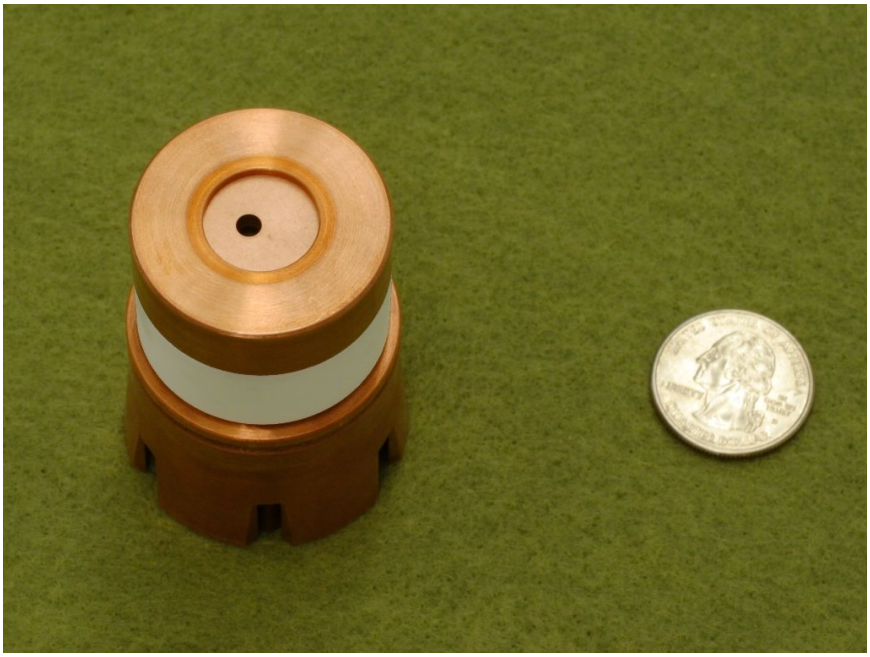

Figure E.5 The cathode cap is tightened onto the trigger disk.

E.2 Mounting Ring Assembly

This section provides assembly instructions for the mounting rings.

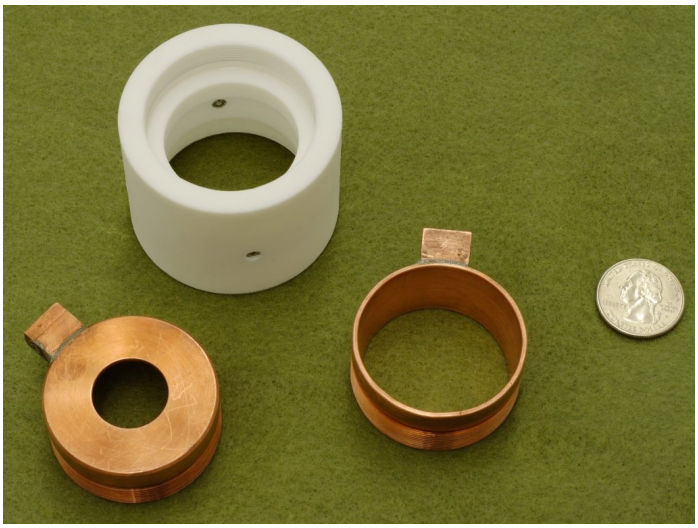

Figure E.6 The individual pieces for the mounting rings.

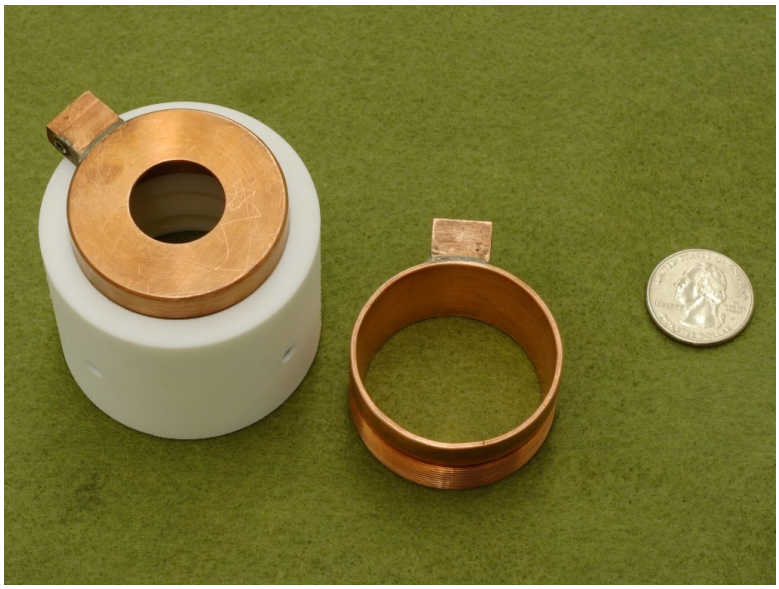

Figure E.7 The trigger ring is threaded into the front of the macor ring.

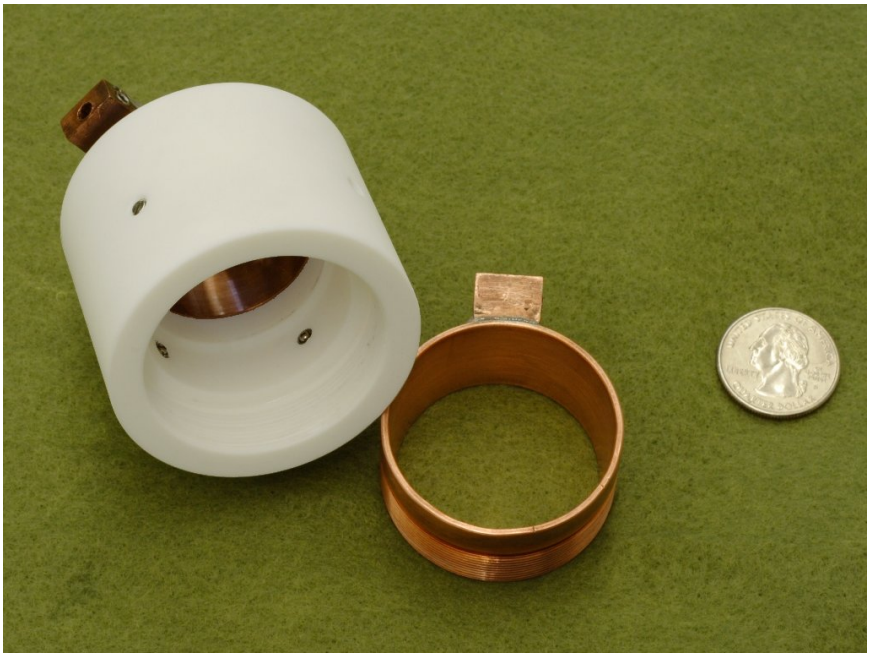

Figure E.8 The ends are not identical—the back side is the one with the spring-loaded bearings, as seen in this picture.

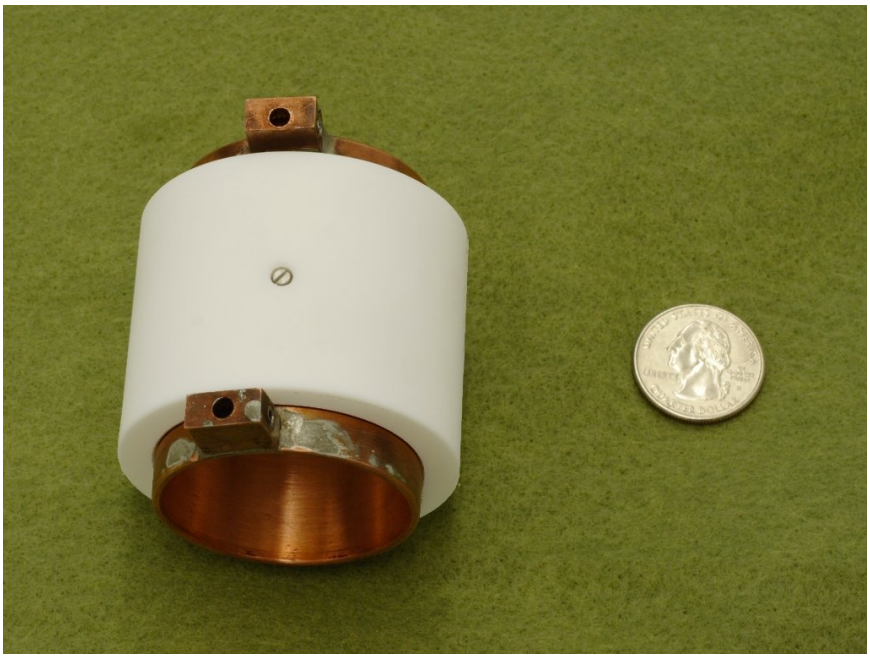

Figure E.9 The cathode ring threads into the back of the macor ring.